Active aero-visco-elastic flutter control and layerwise modelling of supersonic smart sandwich panels with variable stiffness composites

Aerospace Science and Technology 157 (2025) 109847

Contents lists available at ScienceDirect

Aerospace Science and Technology

journal homepage: www.elsevier.com/locate/aescte

Active aero-visco-elastic flutter control and layerwise modelling of supersonic smart sandwich panels with variable stiffness composites

J.A. Moreira [a,*], F. Moleiro [a], A.L. Araújo [a], A. Pagani [b]

[a] IDMEC, Instituto Superior Tecnico, Universidade de Lisboa, Av. Rovisco Pais 1, Lisboa, 1049-001, Portugal
[b] MUL2, Department of Mechanical and Aerospace Engineering, Politecnico di Torino, Corso Duca degli Abruzzi 24, Torino, 10129, Italy

ARTICLE INFO

Communicated by Grigorios Dimitriadis

Keywords:
Aero-visco-elasticity
Active flutter control
Viscoelastic sandwich panels
Variable stiffness composites
Layerwise theory

ABSTRACT

This work focuses on the active aero-visco-elastic flutter control of smart sandwich panels under supersonic airflow by combining viscoelastic materials with variable stiffness composites and surface bonded piezoelectric sensor/actuator layers, exploring variable-order layerwise models based on shear deformation theories. Numerical applications of smart sandwich panels encompass either viscoelastic or purely elastic core, along with elastic layers of composite laminates, using unidirectional or curvilinear fibres, considering thin and moderately thick panels, as well as narrow and wide cores. Proportional and derivative feedback control laws are implemented resorting to the electric potential differences across the piezoelectric layers. Comparing the control laws, it is concluded that the proportional control has a significant stabilizing effect on the occurrence of coupled-mode flutter, as in sandwich panels with purely elastic core, unlike the derivative control. However, when dealing with single mode flutter, as in viscoelastic sandwich panels described with complex modulus approach, the derivative control outperforms the proportional control in improving the flutter resistance. Ultimately, the accuracy assessment of the models predictive capabilities in active flutter control analysis reveals that although the layerwise first-order model ensures a good compromise between numerical accuracy and computational efficiency, especially in thin sandwich panels, high-order models are necessary for moderately thick panels.

1. Introduction

The continuous evolution in material science and structural analysis has played a groundbreaking role in advancing various fields of engineering and related industries. In particular, the aerospace industry has greatly benefited from the advancements in composite materials and sandwich structures, which have paved the way for the development of lightweight and exceptionally efficient aircraft, bringing about significant economic benefits and contributing to environmental sustainability. To be precise, the growth in the production of fibre reinforced composites has led to the emergence of variable stiffness composite (VSC) laminates, with curvilinear fibre paths, as a resourceful and highly promising structural design technology to make progress on the development of advanced composite structures, offering a great potential for buckling resistance enhancement [1], improved vibration response [2] and aeroelastic stability augmentation of both wings [3] and supersonic panels [4]. Furthermore, there is a growing interest in exploring advanced materials that can effectively attenuate mechanical vibrations and aeroelastic instabilities. In fact, smart materials with adaptive multifunctional capabilities, such as piezoelectric materials, are emerging as a promising structural design technology for active vibration control, noise attenuation, and structural health monitoring, as the direct and converse piezoelectric effects provide sensing and actuation capabilities to the structure [5,6]. Since aerospace structures such as wings, control surfaces and fuselage skins are prone to fluid induced vibrations and aeroelastic instabilities, which may result in catastrophic failure or, at least, reduce the operating lifetime due to fatigue, smart structures technology has also found success in active aeroelastic control of wings [7–10] and skin panels [11–16]. Likewise, viscoelastic materials are a cornerstone as far as passive damping treatments are considered for reducing structural vibrations and noise radiation in lightweight sandwich structures [17–19]. Despite the potential stabilizing or destabilizing effects of material damping and viscoelastic damping on panel flutter [20–22], significant aeroelastic improvements are attainable through design optimization of the viscoelastic constraining layer [23–27]. Hence, in light of the increasing demand for the development of high-speed air vehicles exposed to supersonic airflow, such as space launchers, military fighters, and operational unmanned

* Corresponding author.
E-mail address: joao.anjos.moreira@tecnico.ulisboa.pt (J.A. Moreira).

https://doi.org/10.1016/j.ast.2024.109847
Received 18 June 2024; Received in revised form 3 December 2024; Accepted 4 December 2024

Available online 9 December 2024

aerial vehicles (UAVs), a comprehensive understanding of active-passive aeroelastic flutter control technologies in supersonic panels is of crucial relevance to achieve advanced and multifunctional aero-structural engineering systems [28]. In short, this active-passive flutter/vibration control technology is based on the fact that the piezoelectric actuator layers under applied electric potential exhibit in-plane deformations, forcing the base sandwich panel to bend accordingly. Along with that, high transverse shear deformations are induced in the soft core constrained by the stiff elastic layers, thus enhancing the damping capacity of the viscoelastic dissipative material. However, the proper modelling of smart laminated composite sandwich structures with curvilinear fibres, soft viscoelastic core and piezoelectric sensor and actuator layers is indeed a changeling task due to the combination of high through-thickness inhomogeneity of material properties and in-plane variable stiffness, in addition to the coupled electromechanical response, relying mostly on the application of Layerwise (LW) descriptions or pure three-dimensional (3D) finite element (FE) modelling [29–31].

As regards to LW modelling of smart viscoelastic sandwich panels for active-passive vibration control, Boudaoud et al. [32] developed a LW model involving the First-order Shear Deformation Theory (FSDT) for the viscoelastic core, along with the Classical Plate Theory (CPT) for the (isotropic) purely elastic layers and piezoelectric layers. An efficient approach for high-order LW modelling is proposed by Moita et al. [33], considering Reddy's Third-order Shear Deformation Theory (TSDT) for the viscoelastic core and the CPT for the purely elastic and piezoelectric layers. To include the effect of transverse shear deformations beyond the soft viscoelastic core, the LW model proposed by Araújo et al. [34] considers the First-order Shear Deformation Theory (FSDT) for both elastic composite layers and piezoelectric face layers and the TSDT for the core alone. A further extension of this model is presented by Araújo et al. [35] to include thickness stretching effects in the viscoelastic core, which is also applied in the multiobjective design optimization of smart sandwich panels for active noise reduction developed by Araújo and Madeira [6]. In spite of these kinematic refinements, none of the previously mentioned works includes high-order shear deformations theories beyond the viscoelastic core or aeroelastic coupling effects. It is also worth mentioning recent works on the design and analysis of advanced sandwich structures [36–39], functionally graded materials [40,41] and viscoelastic materials [42].

Concerning the coupled electromechanical static and free vibration analysis of piezoelectric composite plates and shells, further refined LW electro-elastic models have been explored making use of Carrera Unified Formulation (CUF) framework, thus allowing the accuracy assessment of various kinematic models, with any expansion-order, in a systematic and hierarchical manner [43,44]. The application and assessment of refined LW models for free vibration and frequency response analysis of viscoelastic sandwich panels have also been carried out using CUF [45,46]. Moreover, D'Ottavio et al. [47] applied the Sublaminate Generalized Unified Formulation (SGUF) for the dynamic analysis of multi-core viscoelastic sandwich panels, highlighting that quasi-3D accuracy can be attained resorting to the assumption of sublaminates, i.e. fewer mathematical layers than physical layers, while requiring a reduced number of degrees of freedom (DOF) compared to purely LW descriptions. Regarding the assessment of refined structural models for static, free vibration, and buckling analysis of purely elastic VSC laminated plates and shells, a considerable volume of literature is already available [48–52], particularly in recent years, with the majority of them focusing on CUF approach. Refined structural models within CUF have also been successfully applied for the analysis of typical aerospace structures, including the dynamic response of thin-walled and open-section wing boxes subjected to different time-dependent loads (e.g. gust loads) [53] and the free vibration analysis of wing structures made of VSC laminates [54].

However, when it comes to aeroelastic flutter analysis of supersonic sandwich panels with viscoelastic damping treatments, the adopted LW models tend to be the simpler ones, assuming the CPT for the skins and the FSDT for the core [23,24] or piecewise linear displacements [25,26]. Therefore, neither high-order transverse shear deformations nor thickness stretching effects are taken into account. Likewise, in the literature regarding active aeroelastic flutter control of supersonic piezoelectric composite plates, the structural models tend to be merely based on Equivalent Single Layer (ESL) descriptions. In fact, the Classical Laminated Plate Theory (CLPT) is the most applied theory in Rayleigh-Ritz formulations aimed for active panel flutter control analysis [55,14,56,57]. As a result, both transverse shear deformations and through-thickness distributions of displacements with zig-zag profile cannot be captured. Nonetheless, some works considered plate elements with ESL descriptions involving the CLPT [11], as well as plate and shell FSDT elements [10]. Furthermore, Oh and Lee [58] focused on the active aeroelastic flutter control of smart laminated cylindrical panels using a first-order LW model. In view of the aerodynamic modelling, it is also worth mentioning that the quasi-steady First-order Piston Theory is indeed the most commonly used aerodynamic model in the context of supersonic panel flutter analysis [28]. Other than that, with the exception of Guimarães et al. [56] and Moreira et al. [57], none of the aforementioned papers explores VSC laminates with curvilinear fibres for enhancing active panel flutter control.

In light of the limited number of available literature on the application of refined structural models aimed for supersonic panel flutter analysis, Moreira et al. [52] provided an assessment of ESL and LW models, considering both variable order shear deformation theories devoid of thickness stretching and variable order theories based on Lagrange z-expansions including thickness stretching, focused on composite laminates with either unidirectional or curvilinear fibres. As far as flutter and buckling analysis of thin panels is considered, it is verified in [52] that the use of LW descriptions does not improve significantly the ESL modelling when high-order shear deformation theories are applied or, instead, a first-order theory accompanied by a carefully selected shear correction factor. Additionally, thickness stretching can be neglected in thin panels, either with unidirectional or curvilinear fibres, but its inclusion along with refinements in transverse shear may be relevant if one considers moderately thick plates. Moreover, Moreira et al. [27] provided a further extension of variable-kinematic ESL and LW models for the supersonic flutter analysis of soft core viscoelastic sandwich panels with metal or laminated composite skins, using unidirectional and curvilinear fibres. As highlighted by Moreira et al. [27], ESL descriptions provide rather deficient estimations on accounting for the soft viscoelastic core, while LW first-order modelling devoid of thickness stretching ensures a fair compromise between numerical accuracy and computational efficiency when considering thin sandwich panels, with either viscoelastic or purely elastic core. More recently, the active aeroelastic flutter control and LW modelling of supersonic smart variable stiffness composite plates is discussed by Moreira et al. [59], highlighting that LW models involving high-order theories are crucial to accurately predict the flutter bounds of panels that experience flutter due to high order modes, as revealed in variable stiffness configurations under certain control conditions, even when considering thin plates.

Based on this concise yet representative literature review, refined structural models that take full advantage of the highly accurate predictive capabilities associated to LW descriptions with high-order kinematic theories remain mostly unexplored for both active and active-passive flutter control of supersonic sandwich panels. Furthermore, it is also perceived that there is still a lack of research on the integration and tailoring of VSC laminates with curvilinear fibres in smart viscoelastic sandwich panels for aeroelastic flutter control purposes. Hence, the present work emerges as a natural extension of the LW models developed by Moreira et al. [52,27,59] for active aero-visco-elastic flutter control analysis of smart variable stiffness laminated composite sandwich panels with piezoelectric sensor and actuator layers. To the best of the authors' knowledge, this is the first work providing an accuracy assessment of LW models aimed for active aero-visco-elastic flutter control analysis of smart sandwich panels under supersonic airflow, while making progress

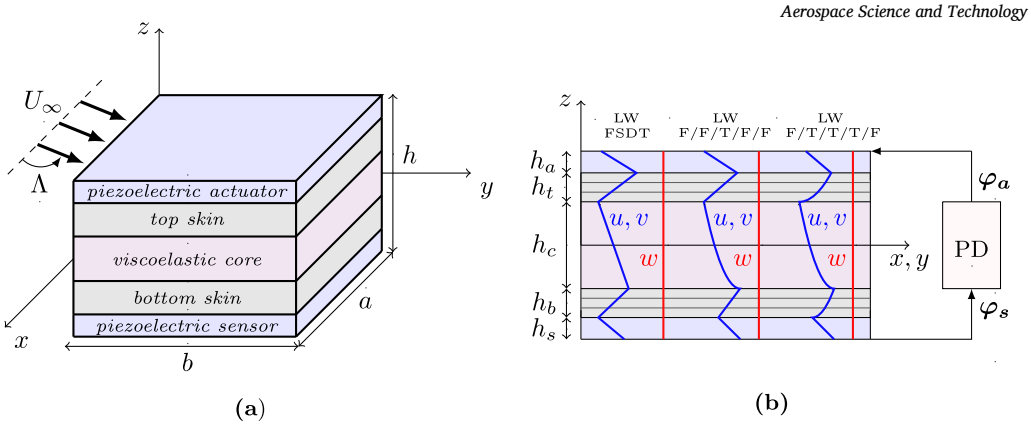

Fig. 1. Illustrative representation of a smart sandwich panel with viscoelastic core, variable stiffness laminated composite skins and surface bonded piezoelectric layers, taken as five discrete layers: (a) under supersonic airflow and (b) connected to a PD control unit and displacements through-thickness distributions involved in the LW models. (For interpretation of the colours in the figure(s), the reader is referred to the web version of this article.)

on the combined application of curvilinear fibre composite laminates, viscoelastic materials and piezoelectric elements as suitable structural design technologies for the development of advanced multifunctional aerospace structures. In more detail, the proposed LW models make use of five discrete layers, where each discrete layer is modelled with variable-order shear deformation theory, either FSDT or TSDT, being progressively refined to render numerical accurate and computational efficient flutter predictions. In line with previous works, the aerodynamic loading is derived by the well-established quasi-steady First-order Piston Theory [20,28,52,27], whereas the viscoelastic behaviour is introduced in the material properties by the complex modulus approach [34,45,27]. The close-loop active control is implemented making use of proportional and derivative feedback control laws, regarding the electric potential differences across the thickness of the transversely-poled piezoelectric sensor/actuator layers, as also followed in [34,14,56,57]. Numerical applications of smart sandwich panels include either viscoelastic or purely elastic core, along with elastic layers made of composite laminates, using unidirectional or curvilinear fibres. The numerical applications are focused on simply supported panels under airflow aligned with the x-axis, encompassing both thin and moderately thick sandwich panels, with either narrow or wide core. For each case, a comprehensive assessment of the models predictive capabilities is provided. Additionally, the impact of proportional and derivative feedback gains, as well as curvilinear fibre tailoring, on the aeroelastic and aero-viscoelastic panel flutter response behaviour is discussed.

2. Layerwise models

The variable-order LW models explored in this work are formulated considering a multilayered panel with a single core and surface bonded piezoelectric layers, taken as a fixed set of five discrete layers - piezoelectric actuator (a), top skin with elastic layers (t), core (c), bottom skin with elastic layers (b) and piezoelectric sensor (s), as illustrated in Fig. 1 - under supersonic airflow on its upper surface with in-plane direction Λ. To provide active control capabilities, the piezoelectric layers are connected to a proportional-derivative (PD) control unit that links the electric potential differences across the thickness of each layer $\boldsymbol{\varphi}_k$. In more detail, it assumed that: (i) the core is made of either viscoelastic or purely elastic material; (ii) each skin can represent a variable stiffness composite laminate with curvilinear fibres, which is a set of elastic layers modelled using an ESL description; and (iii) the piezoelectric materials are polarized in the thickness direction. In Fig. 1, the through-thickness distributions of the in-plane displacements u and v and the transverse displacement w involved in the LW structural models are also illustrated.

As regards to the axiomatic kinematic description of the displacements through-thickness distributions, the intended structural models make use of the FSDT and TSDT at the discrete layer level. Since the total number of discrete layers is fixed, the total number of unknown variables does not depend on the number of actual physical layers within each of the discrete layers. This is indeed a common practice to reduce the computational cost associated to LW descriptions, without impacting significantly the accuracy in terms of global predictive capabilities [47,60,27,59]. More precisely, the FSDT and TSDT assume linear and cubic through-thickness distributions of in-plane displacements u and v, which are described using Taylor z-expansions around the discrete layer mid-plane, along with a constant distribution of the transverse displacement w, thus neglecting transverse normal deformations. In fact, the thickness stretching is disregarded since it plays a minor role when it comes to the supersonic flutter response of thin composite plates [52], which are of primary interest for aerospace applications. This conclusion holds equally for soft core viscoelastic sandwich panels with high through-thickness inhomogeneity of material properties [27], even when considering some cases of moderately thick panels. Furthermore, it is important to mention that while the renowned Koiter recommendations [61] suggest that enhancing the transverse shear deformations would require a simultaneous enrichment in the transverse normal behaviour with respect to thickness stretching, it is worth highlighting that the models based on shear deformation theories devoid of thickness stretching generally possess fewer independent variables in comparison to quasi-3D models that incorporate transverse normal deformations.

Imposing the interlaminar continuity of displacements at the interfaces between adjacent layers [34], the most general case of the LW displacement field involving the TSDT except for the piezoelectric layers, denoted as LW F/T/T/T/F, can be derived as follows:

- *Core layer* ($k = c$):

$$u^c(x,y,z) = u_0^c(x,y) + z\theta_x^c(x,y) + z^2\varkappa_x^c(x,y) + z^3\lambda_x^c(x,y) \tag{1a}$$

$$v^c(x,y,z) = v_0^c(x,y) + z\theta_y^c(x,y) + z^2\varkappa_y^c(x,y) + z^3\lambda_y^c(x,y) \tag{1b}$$

$$w^c(x,y,z) = w_0(x,y) \tag{1c}$$

- *Top skin* ($k = t$):

$$\begin{aligned} u^t(x,y,z) = {} & \alpha_1 u_0^c(x,y) + \alpha_2\theta_x^c(x,y) + \alpha_3\varkappa_x^c(x,y) + \alpha_4\lambda_x^c(x,y) + \\ & \left(\alpha_5 + (z-z_0^t)\right)\theta_x^t(x,y) + \left(\alpha_6 + (z-z_0^t)^2\right)\varkappa_x^t(x,y) + \\ & \left(\alpha_7 + (z-z_0^t)^3\right)\lambda_x^t(x,y) \end{aligned} \tag{2a}$$

$$v^t(x,y,z) = \alpha_1 v_0^c(x,y) + \alpha_2 \theta_y^c(x,y) + \alpha_3 \varkappa_y^c(x,y) + \alpha_4 \lambda_y^c(x,y) + \left(\alpha_5 + (z - z_0^t)\right)\theta_y^t(x,y) + \left(\alpha_6 + (z - z_0^t)^2\right)\varkappa_y^t(x,y) + \left(\alpha_7 + (z - z_0^t)^3\right)\lambda_y^t(x,y) \tag{2b}$$

$$w^t(x,y,z) = w_0(x,y) \tag{2c}$$

- *Bottom skin* ($k = b$):

$$u^b(x,y,z) = \beta_1 u_0^c(x,y) + \beta_2 \theta_x^c(x,y) + \beta_3 \varkappa_x^c(x,y) + \beta_4 \lambda_x^c(x,y) + \left(\beta_5 + (z - z_0^b)\right)\theta_x^b(x,y) + \left(\beta_6 + (z - z_0^b)^2\right)\varkappa_x^b(x,y) + \left(\beta_7 + (z - z_0^b)^3\right)\lambda_x^b(x,y) \tag{3a}$$

$$v^b(x,y,z) = \beta_1 v_0^c(x,y) + \beta_2 \theta_y^c(x,y) + \beta_3 \varkappa_y^c(x,y) + \beta_4 \lambda_y^c(x,y) + \left(\beta_5 + (z - z_0^b)\right)\theta_y^b(x,y) + \left(\beta_6 + (z - z_0^b)^2\right)\varkappa_y^b(x,y) + \left(\beta_7 + (z - z_0^b)^3\right)\lambda_y^b(x,y) \tag{3b}$$

$$w^b(x,y,z) = w_0(x,y) \tag{3c}$$

- *Piezoelectric actuator layer* ($k = a$):

$$u^a(x,y,z) = \alpha_1 u_0^c(x,y) + \alpha_2 \theta_x^c(x,y) + \alpha_3 \varkappa_x^c(x,y) + \alpha_4 \lambda_x^c(x,y) + \gamma_2 \theta_x^t(x,y) + \gamma_4 \lambda_x^t(x,y) + \left(\gamma_5 + (z - z_0^a)\right)\theta_x^a(x,y) \tag{4a}$$

$$v^a(x,y,z) = \alpha_1 v_0^c(x,y) + \alpha_2 \theta_y^c(x,y) + \alpha_3 \varkappa_y^c(x,y) + \alpha_4 \lambda_y^c(x,y) + \gamma_2 \theta_y^t(x,y) + \gamma_4 \lambda_y^t(x,y) + \left(\gamma_5 + (z - z_0^a)\right)\theta_y^a(x,y) \tag{4b}$$

$$w^a(x,y,z) = w_0(x,y) \tag{4c}$$

- *Piezoelectric sensor layer* ($k = s$):

$$u^s(x,y,z) = \beta_1 u_0^c(x,y) + \beta_2 \theta_x^c(x,y) + \beta_3 \varkappa_x^c(x,y) + \beta_4 \lambda_x^c(x,y) + \delta_2 \theta_x^b(x,y) + \delta_4 \lambda_x^b(x,y) + \left(\delta_5 + (z - z_0^s)\right)\theta_x^s(x,y) \tag{5a}$$

$$v^s(x,y,z) = \beta_1 v_0^c(x,y) + \beta_2 \theta_y^c(x,y) + \beta_3 \varkappa_y^c(x,y) + \beta_4 \lambda_y^c(x,y) + \delta_2 \theta_y^b(x,y) + \delta_4 \lambda_y^b(x,y) + \left(\delta_5 + (z - z_0^s)\right)\theta_y^s(x,y) \tag{5b}$$

$$w^s(x,y,z) = w_0(x,y) \tag{5c}$$

where u^k, v^k and w^k are the displacements of the k-discrete layer, with $k = \{a, t, c, b, s\}$, noting that the subscript 0 in the displacements identifies the mid-plane location, i.e. at the mid-plane transverse coordinate z_0^k. Additionally, θ_x^k and θ_y^k represent the rotations of the normals to the mid-plane about the y- and x-axes, respectively, whereas $\varkappa_x^k$, $\varkappa_y^k$, λ_x^k and λ_y^k stand for the higher-order generalized displacements of each k-discrete layer.

In Eqs. (2) to (5), the variables α_n, β_n, γ_n and δ_n are derived from the interlaminar continuity of displacements as shown:

$$\alpha_1 = 1,\ \alpha_2 = h_c/2,\ \alpha_3 = \alpha_2^2,\ \alpha_4 = \alpha_2^3,\ \alpha_5 = h_t/2,\ \alpha_6 = -\alpha_5^2,\ \alpha_7 = \alpha_5^3 \tag{6a}$$

$$\beta_1 = 1,\ \beta_2 = -h_c/2,\ \beta_3 = \beta_2^2,\ \beta_4 = -\beta_2^3,\ \beta_5 = -h_b/2,\ \beta_6 = -\beta_5^2,\ \beta_7 = \beta_5^3 \tag{6b}$$

$$\gamma_2 = h_t,\ \gamma_4 = h_t^3/4,\ \gamma_5 = h_a/2 \tag{6c}$$

$$\delta_2 = -h_b,\ \delta_4 = -h_b^3/4,\ \delta_5 = -h_s/2 \tag{6d}$$

Since the FSDT is a particular case of the high-order shear deformation theories, retaining only constant and linear terms, further LW kinematic descriptions can be deduced from Eqs. (1) to (5). To do so, specific high-order generalized displacements are omitted from the z-expansions of the in-plane displacements. Particularly, the LW model involving the TSDT for the core alone (denoted as LW F/F/T/F/F) is recovered by neglecting the high-order generalized displacements associated to the top and bottom elastic skins (i.e. $k = t$ and b). Furthermore, the LW model which makes sole use of the FSDT (LW FSDT) is obtained by disregarding the high-order terms in all discrete layers. Hence, the most refined model implies a total of twenty five mechanical DOF per node, structured as follows:

$$\boldsymbol{d} = \{u_0^c\ v_0^c\ w_0^c\ \theta_x^c\ \theta_y^c\ \varkappa_x^c\ \varkappa_y^c\ \lambda_x^c\ \lambda_y^c\ \theta_x^t\ \theta_y^t\ \varkappa_x^t\ \varkappa_y^t\ \lambda_x^t\ \lambda_y^t\ \theta_x^b\ \theta_y^b\ \varkappa_x^b\ \varkappa_y^b\ \lambda_x^b\ \lambda_y^b\ \theta_x^a\ \theta_y^a\ \theta_x^s\ \theta_y^s\}^T \tag{7}$$

whereas for the LW model with TSDT for the core alone, only seventeen mechanical DOF remain since the high-order terms of the top and bottom layers are neglected. For the LW FSDT model, no high-order generalized displacement is included and therefore only thirteen mechanical DOF remain.

An additional noteworthy detail regarding the first-order modelling is that a shear correction factor is commonly applied for the evaluation of transverse shear stresses [29]. Nonetheless, in the present LW framework, it is assumed a unit shear correction factor, i.e. $K_s = 1$, which means that no correction is actually applied, as also followed by Moreira et al. [60,50,52]. This is avoided altogether when resorting to the more refined TSDT.

In line with linear electroelasticity, the coupled constitutive equations of an orthotropic and transversely poled piezoelectric layer under plane stress assumptions are written in the global reference system (x, y, z) as shown:

$$\begin{Bmatrix} \sigma_{xx} \\ \sigma_{yy} \\ \sigma_{yz} \\ \sigma_{xz} \\ \sigma_{xy} \end{Bmatrix} = \begin{bmatrix} \bar{Q}_{11} & \bar{Q}_{12} & 0 & 0 & \bar{Q}_{16} \\ \bar{Q}_{12} & \bar{Q}_{22} & 0 & 0 & \bar{Q}_{26} \\ 0 & 0 & \bar{Q}_{44} & \bar{Q}_{45} & 0 \\ 0 & 0 & \bar{Q}_{45} & \bar{Q}_{55} & 0 \\ \bar{Q}_{16} & \bar{Q}_{26} & 0 & 0 & \bar{Q}_{66} \end{bmatrix} \begin{Bmatrix} \varepsilon_{xx} \\ \varepsilon_{yy} \\ \gamma_{yz} \\ \gamma_{xz} \\ \gamma_{xy} \end{Bmatrix} - \begin{bmatrix} 0 & 0 & \bar{e}_{31} \\ 0 & 0 & \bar{e}_{32} \\ \bar{e}_{14} & \bar{e}_{24} & 0 \\ \bar{e}_{15} & \bar{e}_{25} & 0 \\ 0 & 0 & \bar{e}_{36} \end{bmatrix} \begin{Bmatrix} E_x \\ E_y \\ E_z \end{Bmatrix} \tag{8a}$$

$$\begin{Bmatrix} D_x \\ D_y \\ D_z \end{Bmatrix} = \begin{bmatrix} 0 & 0 & \bar{e}_{14} & \bar{e}_{15} & 0 \\ 0 & 0 & \bar{e}_{24} & \bar{e}_{25} & 0 \\ \bar{e}_{31} & \bar{e}_{32} & 0 & 0 & \bar{e}_{36} \end{bmatrix} \begin{Bmatrix} \varepsilon_{xx} \\ \varepsilon_{yy} \\ \gamma_{yz} \\ \gamma_{xz} \\ \gamma_{xy} \end{Bmatrix} + \begin{bmatrix} \bar{\epsilon}_{11} & \bar{\epsilon}_{12} & 0 \\ \bar{\epsilon}_{12} & \bar{\epsilon}_{22} & 0 \\ 0 & 0 & \bar{\epsilon}_{33} \end{bmatrix} \begin{Bmatrix} E_x \\ E_y \\ E_z \end{Bmatrix} \tag{8b}$$

where σ_{ij} are the stresses, ε_{ii} the infinitesimal normal strains, $\gamma_{ij} = 2\varepsilon_{ij}$ the engineering shear strains, D_i the electric displacement and E_i the electric field. The implied material coefficients are the reduced elastic coefficients $\bar{Q}_{ij}$, reduced piezoelectric coefficients $\bar{e}_{ij}$ and reduced dielectric coefficients $\bar{\epsilon}_{ij}$ [29]. For non piezoelectric materials, the piezoelectric coefficients are null and therefore the electro-elastic constitutive equations are decoupled.

Making use of a more convenient compact notation, the reduced plane stress constitutive equations of the p-physical layer within the k-discrete layer are written in the global reference system (x, y, z) as follows:

$$\boldsymbol{\sigma}^{kp} = \bar{\boldsymbol{Q}}^{kp}\boldsymbol{\varepsilon}^{kp} - \bar{\boldsymbol{e}}^{kp}\boldsymbol{E}^{kp} \tag{9a}$$

$$\boldsymbol{D}^{kp} = \bar{\boldsymbol{e}}^{kpT}\boldsymbol{\varepsilon}^{kp} + \bar{\boldsymbol{\epsilon}}^{kp}\boldsymbol{E}^{kp} \tag{9b}$$

Additionally, the linear strain-displacements equations and field-potential equations are provided by:

$$\varepsilon_{ij} = \frac{1}{2}\left(\frac{\partial u_i}{\partial x_j} + \frac{\partial u_j}{\partial x_i}\right) \tag{10a}$$

$$E_i = -\frac{\partial \phi}{\partial x_i} \tag{10b}$$

where $(u_1, u_2, u_3) \equiv (u, v, w)$ are the displacement components in the x-, y- and z-axis, respectively, such that the displacement vector is $\boldsymbol{u} = \{u\ v\ w\}^T$, whereas ϕ is the electric potential.

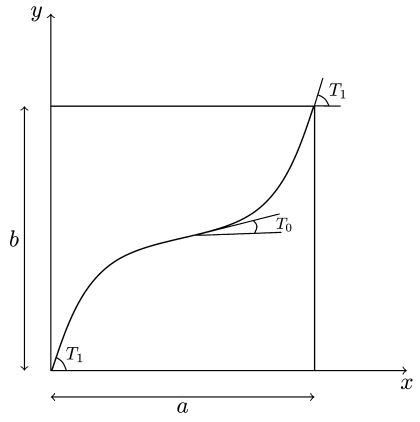

Fig. 2. Variable stiffness composite layer with linear fibre angle distribution $< T_0, T_1 >$ along the x-axis.

Under the common assumption of a linear through-thickness distribution of electric potential, such that it is applied to piezoelectric layers via surface electrodes, the in-plane electric field components are thus null, i.e. $E_x = E_y = 0$. Accordingly, the constant transverse electric field comes out in line with Eq. (10b) as shown:

$$E_z^k = -\frac{\Delta\phi^k}{h^k} \tag{11}$$

where $\Delta\phi^k$ represents the electric potential difference between the upper and lower surfaces of the piezoelectric layer, noting that $\Delta\phi^k = 0$ for non piezoelectric layers.

Due to the necessary in-plane rotation between the layer material reference system and the global reference system [29], it is worth highlighting that when dealing with curvilinear fibre composite layers, the elastic coefficients in the global reference system are given as in-plane continuous functions, i.e. $\bar{\boldsymbol{Q}}^{kp} = \bar{\boldsymbol{Q}}^{kp}(x, y)$, which depend on the fibre angle distribution $\theta^{kp}(x, y)$. More precisely, it is considered that each composite layer assumes a linear fibre angle distribution along the x-axis [50,57], as shown:

$$\theta^{kp}(x) = T_0^{kp} + \frac{2(T_1^{kp} - T_0^{kp})}{a}\left|x - \frac{a}{2}\right| \ , \quad 0 \le x \le a \tag{12}$$

where the control angles $< T_0^{kp}, T_1^{kp} >$ are $T_0^{kp} = \theta^{kp}(a/2)$ and $T_1^{kp} = \theta^{kp}(0) = \theta^{kp}(a)$, as shown in Fig. 2.

Also noteworthy is that in the case of viscoelastic materials, the engineering constants are described using the complex modulus approach. This means that the Young moduli, shear moduli, and Poisson coefficients have both real and imaginary parts, with the imaginary part representing the damping behaviour. Nonetheless, it is common practice to assume no damping associated to the Poisson coefficients, resulting that the engineering constants of viscoelastic isotropic materials are reduced to the complex Young modulus $E = E^*(1 + i\eta)$, with $i = \sqrt{-1}$ and η being the loss factor, and to the real Poisson coefficient ν. Accordingly, the reduced elastic coefficients in Eq. (8a) arise as complex numbers. In the most realistic scenario, the actual mechanical response of viscoelastic materials can be highly non-linear as well as frequency- and temperature-dependent. However, at this preliminary stage, such advanced effects are not explored within the scope of the numerical applications herein.

3. FE formulation and equilibrium equations

The FE formulation is expressed adopting a general notation in matrix form, where the size and elements of the matrices depend on the chosen kinematic theory, as also followed in previous works developed by the authors [60,50,52,27,59]. Therefore, for an arbitrary k-discrete layer, the 1D z-expansions and 2D FE approximations of $\boldsymbol{u}^k$ and $\boldsymbol{\epsilon}^k$ are defined by:

$$\boldsymbol{u}^k = \boldsymbol{Z}^k \boldsymbol{N}^k \boldsymbol{d} \tag{13a}$$

$$\boldsymbol{\epsilon}^k = \boldsymbol{S}^k \boldsymbol{B}^k \boldsymbol{d} \tag{13b}$$

where $\boldsymbol{Z}^k$ and $\boldsymbol{S}^k$ contain the z-expansion functions and their derivatives through the discrete layer thickness, while $\boldsymbol{N}^k$ and $\boldsymbol{B}^k$ define the necessary FE approximations in-plane using 2D shape functions. The adopted 2D shape functions are quadratic Lagrange functions, corresponding to the standard nine-node quadrilateral element [29] (Q9). Thus, the element DOF are structured as $\boldsymbol{d} = \{\boldsymbol{d}_1^T \ \ldots \ \boldsymbol{d}_9^T\}^T$, where $\boldsymbol{d}_j$ represents the nodal DOF. The C^0-interpolation in-plane, as required by the adopted kinematic theories, is then fulfilled by the 2D Lagrange polynomials, thereby maintaining the interelement continuity of primary variables.

In the most general case of multiple piezoelectric patches, the electric potential differences in each patch are altogether structured in the electric potential vector $\boldsymbol{\varphi}^k = \left\{\Delta\phi^{k1} \ \ldots \ \Delta\phi^{kNPP}\right\}^T$ associated to the piezoelectric layers $k = \{a, s\}$, where NPP stands for the number of piezoelectric patches in each side of the panel. Assuming that the piezoelectric layers are covered with surface electrodes, which means equipotential conditions in-plane, the total number of electrical DOF is $\mathcal{N}_e = 2 \times NPP$. In line with Eq. (11), the electric field vector is then defined in terms of the vector of electric potentials as shown:

$$\boldsymbol{E}^k = -\boldsymbol{S}_\phi^k \boldsymbol{B}_\phi^k \boldsymbol{\varphi}^k \tag{14}$$

such that the matrices $\boldsymbol{S}_\phi^k$ and $\boldsymbol{B}_\phi^k$ are the following:

$$\boldsymbol{S}_\phi^k = \left[(\boldsymbol{e}_z)_1 \ \ldots \ (\boldsymbol{e}_z)_{NPP}\right] \tag{15a}$$

$$\boldsymbol{B}_\phi^k = \left(1/h^k\right)\boldsymbol{\mathcal{I}} \tag{15b}$$

where $\boldsymbol{\mathcal{I}}$ represents the identity tensor with dimension $NPP \times NPP$. When dealing with smart sandwich panels fully covered by piezoelectric layers, as in the present numerical applications, a single piezoelectric patch covers the whole surface in each side of the panels, as shown in Fig. 1, which means $NPP = 1$ and $\mathcal{N}_e = 2$.

The Principle of Hamilton is applied to derive the dynamic aero-electro-elastic equilibrium equations of the smart sandwich panels under supersonic airflow on the upper surface ($z = h/2$). Taking the supersonic panels as a set of discrete electro-elastic layers with in-plane surface S and thickness domain h^k, the variational formulation is expressed as follows:

$$\sum_k \int_S \int_{h^k} \delta\boldsymbol{\epsilon}^{kT} \boldsymbol{\sigma}^k - \delta\boldsymbol{E}^{kT} \boldsymbol{D}^k + \rho^k \delta\boldsymbol{u}^{kT} \ddot{\boldsymbol{u}}^k \, dz dS = \int_S \delta\boldsymbol{u}^{aT}|_{\frac{h}{2}} \boldsymbol{e}_z \Delta p \, dS \tag{16}$$

where δ stands for the variational operator, ρ^k is the k-layer density and $\boldsymbol{e}_z = \{0 \ 0 \ 1\}^T$. In addition, the single- and double-dot notations (when used) represent the first and second time derivatives, respectively.

On the right-hand side of Eq. (16), the aerodynamic loading Δp generated by the airflow is assumed to be described according to the well-known 2D quasi-steady First-order Supersonic Piston Theory, which is a simple formulation that provides accurate results in the high supersonic range [20,28]. Considering airflow with yaw angle Λ, as shown in Fig. 1, the distributed transverse pressure predicted by the 2D quasi-steady First-order Supersonic Piston Theory is defined by:

$$\Delta p = -\lambda\left(\frac{\partial w}{\partial x}\cos\Lambda + \frac{\partial w}{\partial y}\sin\Lambda\right) - g_a \frac{\partial w}{\partial t} \tag{17}$$

such that the dynamic pressure parameter λ and aerodynamic damping g_a are expressed in terms of the airflow properties as shown:

$$\lambda = \frac{\rho_\infty U_\infty^2}{\sqrt{M_\infty^2 - 1}} \tag{18a}$$

$$g_a = \frac{\lambda}{U_\infty} \frac{(M_\infty^2 - 2)}{(M_\infty^2 - 1)} \tag{18b}$$

where ρ_∞, U_∞ and M_∞ represent the density, speed and Mach number of the free airflow.

Introducing the approximations given in Eqs. (13) and (14), the constitutive relations in Eqs. (9) as well as the aerodynamic pressure distribution in Eq. (17), all together, into Eq. (16), gives rise to the FE equilibrium equations. These equations can then be written separating the electrical DOF of the sensor and actuator layers as follows:

$$\boldsymbol{M}_{uu}\ddot{\boldsymbol{d}} + g_a \boldsymbol{C}_{\Delta p}\dot{\boldsymbol{d}} + (\boldsymbol{K}_{uu} + \lambda \boldsymbol{K}_{\Delta p})\boldsymbol{d} + \boldsymbol{K}^a_{u\phi}\boldsymbol{\varphi}^a + \boldsymbol{K}^s_{u\phi}\boldsymbol{\varphi}^s = \boldsymbol{0} \tag{19a}$$

$$\boldsymbol{K}^{a^T}_{u\phi}\boldsymbol{d} + \boldsymbol{K}^a_{\phi\phi}\boldsymbol{\varphi}^a = \boldsymbol{0} \tag{19b}$$

$$\boldsymbol{K}^{s^T}_{u\phi}\boldsymbol{d} + \boldsymbol{K}^s_{\phi\phi}\boldsymbol{\varphi}^s = \boldsymbol{0} \tag{19c}$$

where $\boldsymbol{M}_{uu}$, $g_a\boldsymbol{C}_{\Delta p}$, $\boldsymbol{K}_{uu}$, $\lambda\boldsymbol{K}_{\Delta p}$, $\boldsymbol{K}^k_{u\phi}$ and $\boldsymbol{K}^k_{\phi\phi}$ are the mass, aerodynamic damping, purely elastic stiffness, aerodynamic stiffness, electromechanical coupling stiffness and dielectric stiffness matrices of the finite element, respectively. Recalling that, in the most general case, each k-discrete layer can represent a sublaminate consisting of N_p^k physical layers, with $k = \{a, t, c, b, s\}$, the implied FE matrices are expressed by:

$$\boldsymbol{M}_{uu} = \sum_k \sum_{p=1}^{N_p^k} \int_\Omega \boldsymbol{N}^{k^T} \left(\int_{h^{kp}} \rho^{kp} \boldsymbol{Z}^{k^T} \boldsymbol{Z}^k dz \right) \boldsymbol{N}^k d\Omega \tag{20a}$$

$$\boldsymbol{K}_{uu} = \sum_k \sum_{p=1}^{N_p^k} \int_\Omega \boldsymbol{B}^{k^T} \left(\int_{h^{kp}} \boldsymbol{S}^{k^T} \bar{\boldsymbol{Q}}^{kp} \boldsymbol{S}^k dz \right) \boldsymbol{B}^k d\Omega \tag{20b}$$

$$\boldsymbol{K}^k_{u\phi} = \sum_{p=1}^{N_p^k} \int_\Omega \boldsymbol{B}^{k^T} \left(\int_{h^{kp}} \boldsymbol{S}^{k^T} \bar{\boldsymbol{e}}^{kp} \boldsymbol{S}^k_\phi dz \right) \boldsymbol{B}^k_\phi d\Omega \tag{20c}$$

$$\boldsymbol{K}^k_{\phi\phi} = \sum_{p=1}^{N_p^k} \int_\Omega \boldsymbol{B}^{k^T}_\phi \left(\int_{h^{kp}} \boldsymbol{S}^{k^T}_\phi \bar{\boldsymbol{\epsilon}}^{kp} \boldsymbol{S}^k_\phi dz \right) \boldsymbol{B}^k_\phi d\Omega \tag{20d}$$

$$\boldsymbol{C}_{\Delta p} = \int_\Omega \boldsymbol{N}^{a^T} \boldsymbol{Z}^{a^T} |_{\frac{h}{2}} \boldsymbol{e}_z \boldsymbol{e}_z^T \boldsymbol{Z}^a |_{\frac{h}{2}} \boldsymbol{N}^a d\Omega \tag{20e}$$

$$\boldsymbol{K}_{\Delta p} = \int_\Omega \boldsymbol{N}^{a^T} \boldsymbol{Z}^{a^T} |_{\frac{h}{2}} \boldsymbol{e}_z \boldsymbol{e}_z^T \boldsymbol{Z}^a |_{\frac{h}{2}} \left(\frac{\partial \boldsymbol{N}^a}{\partial x} \cos\Lambda + \frac{\partial \boldsymbol{N}^a}{\partial y} \sin\Lambda \right) d\Omega \tag{20f}$$

It is worth mentioning that the 1D integrals in each thickness domain h^{kp} are evaluated using exact integration, whereas the integration in the in-plane FE domain Ω is carried out numerically with Gauss quadrature. To prevent shear locking effects [29], it is considered reduced integration for the shear terms of the stiffness matrix given in Eq. (20b). In fact, due to the complex modulus approach adopted to describe the viscoelastic material properties, the stiffness matrix $\boldsymbol{K}_{uu}$ stated in Eq. (20b) ends up complex when dealing with viscoelastic sandwich panels. Furthermore, in the case of variable stiffness composite layers with curvilinear fibres, the fibre angle is evaluated at each integration point to enhance the accuracy of the elastic coefficients.

4. Active aero-visco-elastic flutter control

Once the standard FE assembly of the element equilibrium equations, as specified in Eq. (19), and the imposition of boundary conditions have been carried out, the active control is then implemented resorting to the global system matrices [59]. From the equation associated to the electrical DOF of the sensor layer, the electric potential difference across the piezoelectric sensor comes out as shown:

$$\boldsymbol{\varphi}^s = -\boldsymbol{K}^{s^{-1}}_{\phi\phi}\boldsymbol{K}^{s^T}_{u\phi}\boldsymbol{\Delta} \tag{21}$$

where $\boldsymbol{\Delta}$ stands for the global mechanical DOF.

In view of the close-loop proportional-derivative feedback control law, the electric potential applied to the piezoelectric actuator is given by:

$$\boldsymbol{\varphi}^a = G_p\boldsymbol{\varphi}^s + G_d\dot{\boldsymbol{\varphi}}^s \tag{22}$$

which is related to the mechanical DOF $\boldsymbol{\Delta}$ and their time derivatives $\dot{\boldsymbol{\Delta}}$ by means of Eq. (21), as follows:

$$\boldsymbol{\varphi}^a = -G_p\boldsymbol{K}^{s^{-1}}_{\phi\phi}\boldsymbol{K}^{s^T}_{u\phi}\boldsymbol{\Delta} - G_d\boldsymbol{K}^{s^{-1}}_{\phi\phi}\boldsymbol{K}^{s^T}_{u\phi}\dot{\boldsymbol{\Delta}} \tag{23}$$

where G_p and G_d are the proportional and derivative feedback gains, respectively.

Introducing Eqs. (21) and (23) in the global system of equilibrium equations, the active aero-visco-elastic equilibrium equations end up decoupled, as shown:

$$\boldsymbol{M}_{uu}\ddot{\boldsymbol{\Delta}} + (\boldsymbol{C}^* + g_a\boldsymbol{C}_{\Delta p})\dot{\boldsymbol{\Delta}} + (\boldsymbol{K}^* + \lambda\boldsymbol{K}_{\Delta p})\boldsymbol{\Delta} = \boldsymbol{0} \tag{24}$$

where the active damping matrix $\boldsymbol{C}^*$ and condensed stiffness matrix $\boldsymbol{K}^*$ are derived as follows:

$$\boldsymbol{C}^* = -G_d\boldsymbol{K}^a_{u\phi}\boldsymbol{K}^{s^{-1}}_{\phi\phi}\boldsymbol{K}^{s^T}_{u\phi} \tag{25a}$$

$$\boldsymbol{K}^* = \boldsymbol{K}_{uu} - (G_p\boldsymbol{K}^a_{u\phi} + \boldsymbol{K}^s_{u\phi})\boldsymbol{K}^{s^{-1}}_{\phi\phi}\boldsymbol{K}^{s^T}_{u\phi} \tag{25b}$$

Under the assumption of harmonic solutions in the form of $\boldsymbol{\Delta} = \hat{\boldsymbol{\Delta}}e^{s_n t}$, the characteristic equation of the global (quadratic) eigenvalue problem is given by:

$$\left| s_n^2\boldsymbol{M}_{uu} + s_n(\boldsymbol{C}^* + g_a\boldsymbol{C}_{\Delta p}) + \boldsymbol{K}^* + \lambda\boldsymbol{K}_{\Delta p} \right| = 0 \tag{26}$$

where the dynamic pressure parameter λ and aerodynamic damping g_a depend on the airflow conditions according to Eq. (18). In addition, for Short Circuit (SC) conditions of the surface electrodes, the electric potentials are null, i.e. $\boldsymbol{\varphi}^s = \boldsymbol{\varphi}^a = 0$, and therefore $\boldsymbol{K}^* = \boldsymbol{K}_{uu}$ and $\boldsymbol{C}^* = \boldsymbol{0}$. The SC conditions are herein considered as representative of an uncontrolled system, whereas for any non zero control gain G_p or G_d, the active control system is considered to be operational.

In the absence of active and aerodynamic damping terms in Eq. (26), the characteristic equation of the linear eigenvalue problem takes the standard form, as shown:

$$\left| s_n^2\boldsymbol{M}_{uu} + \boldsymbol{K}^* + \lambda\boldsymbol{K}_{\Delta p} \right| = 0 \tag{27}$$

noting that the particular case of free vibration in vacuum is recovered by assuming $\lambda = 0$.

When the active and/or aerodynamic damping terms are taken into account, the quadratic eigenvalue problem stated in Eq. (26) can be solved as a linear problem, with a dimension that is double of the original one, by adopting a state space format equivalent to Eq. (24), represented as follows [62]:

$$\boldsymbol{\mathcal{A}} \begin{Bmatrix} \dot{\boldsymbol{\Delta}} \\ \ddot{\boldsymbol{\Delta}} \end{Bmatrix} + \boldsymbol{\mathcal{B}} \begin{Bmatrix} \boldsymbol{\Delta} \\ \dot{\boldsymbol{\Delta}} \end{Bmatrix} = \boldsymbol{0} \tag{28}$$

where the symmetric state space matrices $\boldsymbol{\mathcal{A}}$ and $\boldsymbol{\mathcal{B}}$ come out as shown:

$$\boldsymbol{\mathcal{A}} = \begin{bmatrix} \boldsymbol{C}^* + g_a\boldsymbol{C}_{\Delta p} & \boldsymbol{M}_{uu} \\ \boldsymbol{M}_{uu} & \boldsymbol{0} \end{bmatrix} \tag{29a}$$

$$\boldsymbol{\mathcal{B}} = \begin{bmatrix} \boldsymbol{K}^* + \lambda\boldsymbol{K}_{\Delta p} & \boldsymbol{0} \\ \boldsymbol{0} & -\boldsymbol{M}_{uu} \end{bmatrix} \tag{29b}$$

In view of the state space given in Eq. (28), the characteristic equation of the resulting linear eigenvalue problem is the following:

$$|s_n \boldsymbol{A} + \boldsymbol{B}| = 0 \tag{30}$$

where the $2\mathcal{N}$ complex eigenvalues (where $\mathcal{N}$ is the total number of DOF) emerge as complex conjugated pairs $s_n = -\omega_n \xi_n \pm i\omega_d$, with $\omega_d = \omega_n \sqrt{1-\xi_n^2}$ being the damped frequency. Hence, for a given flow condition, the solution of the eigenvalue problem yields the natural frequencies (ω_n) and modal loss factors (ξ_n).

In short, the main objective of the linear aeroelastic flutter stability analysis is the evaluation of the lowest dynamic pressure parameter λ, known as critical flutter pressure parameter λ_F, for which the system becomes dynamically unstable, i.e. with at least one negative modal loss factor ($\xi_n < 0$). Disregarding the aerodynamic and active damping contributions, in addition to the viscoelastic damping, the modal loss factors are null prior to the occurrence of flutter and a perfect coalescence of two natural frequencies arises as flutter occurs. This type of flutter involving coupled modes is the most common and well-explored flutter mechanism and it is usually known as coupled-mode flutter [20]. Regardless of the aerodynamic and active damping effects, when considering the damping resulting from the complex modulus approach that describes the behaviour of the viscoelastic core, a second type of flutter is observed without any coupling of vibration modes [27], thus named single mode flutter [20]. In this case, the modal loss factors are higher than zero prior to the flutter bound, even when considering free vibration in vacuum, and clear transition between the stable region ($\xi_n > 0$) and unstable region ($\xi_n < 0$) is verified as flutter occurs. As a result, the sign of the real part of the eigenvalue that leads to flutter instability changes from positive to negative. These two types of flutter are discussed further in the numerical applications, illustrating the evolution of the natural frequencies and modal loss factors with the dynamic pressure parameter.

5. Numerical applications

The numerical applications are focused on the supersonic flutter analysis and active control of simply supported smart sandwich panels made of either a purely elastic or viscoelastic soft core, along with elastic composite layers and surface bonded piezoelectric sensor/actuator layers covering the whole panel. Subsection 5.1 regards the validation of the developed LW models with available literature solutions and it also includes the convergence analysis results for a representative example of the test cases intended in the present work. In the subsequent subsections, the proposed LW models predictive capabilities are assessed and compared through selected numerical applications, which intentionally consider the following two scenarios: (i) sandwich panels with purely elastic core in Subsection 5.2; and (ii) sandwich panels with viscoelastic core in Subsection 5.3. In addition, for each scenario, the impact of the proportional and derivative feedback control laws on the aeroelastic and aero-visco-elastic flutter response of supersonic smart sandwich panels is discussed in detail.

For numerical applications purposes, the intended smart sandwich panels are idealized as square plates with fixed in-plane dimensions $a = b = 1$ m and a total thickness h adjusted to represent different side-to-thickness ratios, namely, $a/h = 250$, 100, 50 and 20, i.e. from thin to moderately thick plates, respectively, such that more complicated effects may be triggered in the aero-visco-elastic response behaviour of the sandwich panels. As regards to the thickness layouts, it is assumed that each piezoelectric layer has $0.05h$ of thickness, whereas the core can be either narrow or wide depending on the adopted value of core thickness ratio $h_c/h = 0.2$ or 0.8, respectively. Hence, the remaining thickness is equally distributed between the two laminated elastic layers, which are composed by three equal thickness layers as in constant stiffness composite (CSC) laminates with unidirectional fibres or VSC laminates with curvilinear fibres (Eq. (12)). Taking into account three different fibre configurations of the elastic layers, which have been systematically explored in previous works [50,57,52,27], the complete stacking sequences of the symmetric smart sandwich panels are the following:

- *CSC elastic layers*: (PZT-4/0/90/0/core/0/90/0/PZT-4)
- *VSC1 elastic layers*: (PZT-4/<0,45>/<-45,-60>/<0,45>/core/<0,45>/<-45,-60>/<0,45>/PZT-4)
- *VSC2 elastic layers*: (PZT-4/<30,0>/<45,90>/<30,0>/core/<30,0>/<45,90>/<30,0>/PZT-4)

The material properties of the piezoelectric layers, as a transversely isotropic and thickness poled PZT-4, are $E_1 = E_2 = 81.3$ GPa, $E_3 = 64.5$ GPa, $G_{12} = 30.6$ GPa, $G_{13} = G_{23} = 25.6$ GPa, $\nu_{12} = 0.329$, $\nu_{13} = \nu_{23} = 0.432$, $e_{31} = e_{32} = -5.20$ C/m^2, $e_{33} = 15.08$ C/m^2, $e_{15} = e_{24} = 12.72$ C/m^2, $\epsilon_{11} = \epsilon_{22} = 1475\epsilon_0$, $\epsilon_{33} = 1300\epsilon_0$ ($\epsilon_0 = 8.85 \times 10^{-12}$ F/m) and $\rho = 7500$ kg/m^3, whereas the material properties of the elastic layers, as an (orthotropic) graphite-epoxy fibre reinforced composite, are $E_1 = 25E_0$, $E_2 = E_3 = E_0$, $G_{12} = G_{13} = 0.5E_0$, $G_{23} = 0.2E_0$, $\nu_{12} = \nu_{13} = \nu_{23} = 0.25$ and $\rho = 1600$ kg/m^3, where $E_0 = 7$ GPa. In addition, the material properties of the soft core, as an (isotropic) polymer described by a constant viscoelastic model, are $E = 2.67008(1 + i\eta_c)$ MPa, $\eta_c = 0.5$, $\nu = 0.49$ and $\rho = 999$ kg/m^3 [34,27]. In Subsection 5.2, the viscoelastic behaviour of the core is neglected, which means $\eta_c = 0$, since it is exclusively focused on sandwich panels with purely elastic core.

To be clear, the simply supported boundary conditions imposed, at the discrete layer level, are as follows:

$$u^k = w^k = 0 \text{ at } y = 0, b \tag{31a}$$

$$v^k = w^k = 0 \text{ at } x = 0, a \tag{31b}$$

Concerning the electrical conditions (E.C.), the SC conditions of the surface electrodes ($\boldsymbol{\varphi}^s = \boldsymbol{\varphi}^a = 0$) represent the uncontrolled system. For any non zero control gain, either proportional or derivative, the active control system is operational and the electrical potential conditions are established by Eq. (22). Although the units of the control gains are not specified in the numerical applications, it should be emphasized that the proportional feedback gain G_p is dimensionless and the derivative feedback gain G_d is expressed in seconds (s), using S.I. units.

The flutter pressure parameters λ_F are obtained assuming that the airflow is aligned with the x-axis, i.e. yaw angle $\Lambda = 0°$ (Fig. 1), being provided in the following nondimensionalized form:

$$\tilde{\lambda}_F = \frac{\lambda_F a^3}{h^3 G_{12}^c} \tag{32}$$

where G_{12}^c stands for the shear modulus G_{12} of the composite material.

In addition, the flutter solutions presented in this work are obtained neglecting the effect of the aerodynamic damping. Since the aerodynamic damping has mostly a stabilizing impact on the occurrence of supersonic panel flutter [20,22], leading to slightly higher flutter pressure parameters, this assumption is indeed a common practice in the literature [57,52,27]. Hence, from the design point of view, setting $g_a = 0$ in Eq. (29) ensures more conservative flutter analyses.

5.1. Validation and convergence analysis

To provide a validation of the proposed LW models with available literature solutions concerning supersonic flutter analysis of viscoelastic sandwich panels, Table 1 includes a comparison with the results reported by Moreira et al. [27]. It is considered both thin and moderately thick symmetric panels, with metal or curvilinear fibre composite skins (<0,45>/<-45,-60>/<0,45>). The in-plane dimensions are $a = 348$ mm and $b = 304.8$ mm, while the total thickness is either $h = h_0 = 1.778$ mm ($a/h \approx 196$) or $h = 4h_0$ ($a/h \approx 49$). In line with the original benchmark [27], the material properties of the metal skins, as an isotropic aluminium alloy, are $E = 68.9$ GPa, $\nu = 0.3$ and $\rho = 2740$ kg/m^3, whereas the material properties of the composite material are $E_1 = 173$ GPa, $E_2 = E_3 = 7.20$ GPa, $G_{12} = G_{13} = G_{23} = 3.76$ GPa, $\nu_{12} = \nu_{13} = \nu_{23} = 0.29$ and $\rho = 1540$ kg/m^3. Additionally, the properties of the viscoelastic core are the same as considered in the present work and the core thickness

Table 1
Nondimensionalized flutter pressure parameters $\tilde{\lambda}_F$ of viscoelastic sandwich panels with metal or VSC skins, considering thin and moderately thick panels with $h = h_0$ and $4h_0$, respectively: comparison with available literature solutions.

	Metal skins		VSC skins	
Model	$h = h_0$	$h = 4h_0$	$h = h_0$	$h = 4h_0$
LW FSDT [27]	235.26	138.06	231.48	105.44
LW TSDT [27]	235.26	138.04	231.30	105.32
LW Lag3 [27]	235.26	138.19	231.34	105.40
LW FSDT	235.27	138.07	231.33	105.39
LW F/F/T/F/F	235.27	138.07	231.33	105.39
LW F/T/T/T/F	235.27	138.06	231.30	105.32

ratio is $h_c/h = 1/7$. It is assumed simply supported boundary conditions and airflow aligned with the x-axis.

Since there is no piezoelectric face layers in the sandwich panels considered in [27], the five mathematical layers of the proposed LW models need to be adjusted to represent the intended stacking sequences with either three or seven physical/material layers. In view of the LW modelling, the viscoelastic core is represented by the middle discrete layer of the models, whereas each metal skin is modelled using two discrete layers. For the case of 3-layer composite skins, the outer layer and the two inner layers are treated as two discrete layers adjacent to each side of the core. Note that the LW models adopted by Moreira et al. [27] involve solely three discrete layers and, therefore, each skin is treated as an ESL in the case of laminated composite skins. Other than that, the benchmark solutions encompass LW kinematic descriptions devoid of thickness stretching, making use of the FSDT and TSDT for each discrete layer (LW FSDT or LW TSDT, respectively), as well as a further refined quasi-3D model, including through-thickness transverse normal deformation effects, developed based on third-order Lagrange z-expansions of the displacements, thus denoted as the LW Lag3 model. The solutions are obtained making use of 10×10 Q9 elements [27]. Comparing the results provided in Table 1, it is verified that the nondimensionalized flutter pressure parameters predicted by the present models are in good agreement with the literature solutions. This conclusion holds for both types of skin layers as well as for both thin and moderately thick panels, thus validating the developed LW models for flutter analysis of viscoelastic sandwich panels.

Regarding active flutter control, the validation of the proposed LW models is carried out by comparison with available literature solutions by Song et al. [14] and Moreira et al. [59], which are obtained using a Rayleigh-Ritz model involving the CLPT and trigonometric trial functions. The test case consists of a simply supported laminated composite panel with unidirectional fibres at 0°, which is fully covered by piezoelectric face layers and under supersonic airflow along the x-axis. The in-plane dimensions are $a = b = 0.1$ m and the total thickness is $h = 0.0012$ m, with each piezoelectric layer having 0.0001 m of thickness. Additionally, the aerodynamic damping is included and three distinct electrical conditions are investigated, namely: (i) SC; (ii) only proportional feedback gain $G_p = 27.9822$; and (iii) only derivative feedback gain $G_d = 0.0005$. To be precise, the reference solutions for the first two conditions are presented explicitly in [14,59], although for the case of derivative feedback gain, an additional solution is provided in the interest of the present work, thus here made available for the first-time using the Rayleigh-Ritz CLPT model introduced in [57,59]. The present LW solutions are obtained using 10×10 Q9 elements, providing the nondimensionalized flutter pressure parameter in line with the original benchmark [14], i.e. $\tilde{\lambda}_F = \lambda_F a^3/D_1$, where $D_1 = E_1^c h_c^3/(12(1 - \nu_{12}^c \nu_{21}^c))$. The numerical results shown in Table 2 reveal that the present models solutions are in good agreement with the reference solutions, including both proportional and derivative feedback control laws.

In Table 3, the convergence analysis results of the LW FSDT model are provided, considering both free vibration in vacuum and flutter analysis of the smart viscoelastic sandwich panel with *VSC1* elastic layers and narrow core ($h_c/h = 0.2$), considering $a/h = 250$. In more detail, the first six natural frequencies $f_n = \omega_n/(2\pi)$ and corresponding modal loss factors ξ_n are considered in free vibration analysis, whereas the nondimensionalized flutter pressure parameter $\tilde{\lambda}_F$ is presented for the aeroelastic flutter analysis. Moreover, the convergence study is carried out for both SC conditions and derivative control conditions, using a value of $G_d = 0.1$. It is important to highlight that flutter occurs due to the first mode under SC conditions, while under active derivative control conditions with $G_d = 0.1$, flutter is induced by the second mode. Since it is considered a panel with viscoelastic core, flutter occurs due to a single mode rather than being a result of the interaction between two modes [27], as illustrated in the following subsections.

Table 2
Nondimensionalized flutter pressure parameters $\tilde{\lambda}_F$ of a smart composite panel with unidirectional fibres at 0°: comparison with available literature solutions.

Model	SC	$G_p = 27.9822$	$G_d = 0.0005$
CLPT [14]	542.0	789.0	–
CLPT [59]	542.0	789.0	471.0
LW FSDT	541.4	788.8	470.5
LW F/F/T/F/F	541.3	788.6	470.2
LW F/T/T/T/F	541.1	788.5	470.0

The numerical results presented in Table 3 show that the first six natural frequencies and modal loss factors, as well as the nondimensionalized flutter pressure parameters, converge for meshes with more than 10×10 Q9 elements, regardless of the electrical conditions. Nonetheless, it is worth mentioning that the convergence of the nondimensionalized flutter pressure parameter is slower when considering $G_d = 0.1$ since flutter occurs due to the second mode instead of the first mode. Therefore, a mesh with 10×10 Q9 elements is chosen for subsequent flutter analyses in order to ensure the necessary numerical accuracy, while maintaining fast and computationally efficient flutter predictions. It is important to note that similar convergence trends are observed for the other kinematic models, and the mode shapes also converge. By adopting the same FE mesh for all LW models, the accuracy assessment is just focused on the influence of the refinements introduced in the z-expansions of displacements.

5.2. Smart sandwich panels with purely elastic core

For the accuracy assessment of the LW models predictive capabilities in supersonic flutter analysis of smart sandwich panels with purely elastic core, Table 4 presents the nondimensionalized flutter pressure parameters $\tilde{\lambda}_F$ and flutter frequencies f_F (which are defined as the frequency value for which the natural frequencies coalesce at the flutter bound), as well as the modes involved in the occurrence of flutter, considering both unidirectional and curvilinear fibre elastic layers. In addition, the results are provided for both thin and moderately thick plates, assuming a narrow core with a fixed core thickness ratio $h_c/h = 0.2$, while considering either SC conditions of the surface electrodes or active proportional control conditions. Actually, the proportional feedback gains G_p are selected such that the maximum flutter resistance is achieved when considering thin panels with $a/h = 250$.

According to Fig. 3, the maximum nondimensionalized flutter pressure parameters of the thin sandwich panels with $a/h = 250$ and $h_c/h = 0.2$ are obtained when applying: (i) $G_p = 4$ for the case of cross-ply elastic layers; and (ii) $G_p = 11$ for both cases of elastic composite layers with curvilinear fibres. The previously mentioned control gains lead to relative increases of 5% (*CSC*), 35% (*VSC1*) and 38% (*VSC2*) with respect to the nondimensionalized flutter pressure parameter of the corresponding uncontrolled system in SC conditions.

In view of the models accuracy assessment for the analysis of thin sandwich panels, Table 4 reveals that the flutter bounds and flutter frequencies predicted by the three LW models coincide for most test cases

Table 3
Convergence analysis results of the LW FSDT model: first six natural frequencies f_n (Hz), modal loss factors ξ_n (%) and nondimensionalized flutter pressure parameter $\tilde{\lambda}_F$ of the smart viscoelastic sandwich panel with *VSC1* elastic layers ($a/h = 250$, $h_c/h = 0.2$ and $\eta_c = 0.5$) under short circuit (SC) conditions or active derivative control $G_d = 0.1$.

E.C.	Mesh	f_1	ξ_1	f_2	ξ_2	f_3	ξ_3	f_4	ξ_4	f_5	ξ_5	f_6	ξ_6	$\tilde{\lambda}_F$
SC	4×4	16.90	9.10	32.02	10.90	36.07	10.60	48.47	11.34	53.70	11.65	64.85	9.28	238.7
	6×6	16.89	9.08	31.89	10.88	35.87	10.61	48.23	11.39	52.54	11.63	62.66	9.35	238.8
	8×8	16.89	9.08	31.86	10.88	35.84	10.61	48.18	11.40	52.33	11.62	62.34	9.39	238.7
	10×10	16.89	9.08	31.86	10.88	35.83	10.61	48.17	11.40	52.27	11.62	62.25	9.40	238.7
	12×12	16.89	9.08	31.85	10.88	35.82	10.61	48.16	11.41	52.24	11.62	62.22	9.40	238.7
$G_d = 0.1$	4×4	16.88	16.94	32.02	10.90	36.07	10.60	48.55	11.40	53.32	15.70	63.38	12.17	368.6
	6×6	16.87	16.92	31.89	10.88	35.87	10.61	48.31	11.46	52.24	15.10	62.02	11.94	364.5
	8×8	16.87	16.92	31.86	10.88	35.84	10.61	48.26	11.48	52.03	15.00	61.73	11.90	363.8
	10×10	16.87	16.92	31.86	10.88	35.83	10.61	48.25	11.48	51.97	14.98	61.64	11.89	363.6
	12×12	16.87	16.92	31.85	10.88	35.82	10.61	48.24	11.48	51.94	14.97	61.61	11.89	363.5

Table 4
Nondimensionalized flutter pressure parameters $\tilde{\lambda}_F$ and flutter frequencies f_F (Hz) of smart sandwich panels with purely elastic core ($h_c/h = 0.2$, $\eta_c = 0$), considering unidirectional or curvilinear fibre elastic layers, under SC conditions or active proportional control G_p.

			$a/h = 250$		$a/h = 100$		$a/h = 50$		$a/h = 20$	
Case	E.C.	Model	$\tilde{\lambda}_F$	f_F	$\tilde{\lambda}_F$	f_F	$\tilde{\lambda}_F$	f_F	$\tilde{\lambda}_F$	f_F
CSC	SC	LW FSDT	413.0	32.89	206.5	56.32	173.4	99.89	158.4	236.41
		LW F/F/T/F/F	413.0	32.89	206.5	56.32	173.4	99.89	158.4	236.41
		LW F/T/T/T/F	413.0	32.89	206.4	56.32	173.0	99.82	156.0	235.25
	$G_p = 4$	LW FSDT	435.4	33.46	212.5	56.63	177.2	100.27	161.8	237.45
		LW F/F/T/F/F	435.4	33.46	212.5	56.63	177.2	100.27	161.8	237.45
		LW F/T/T/T/F	435.4	33.46	212.4	56.62	176.8	100.21	159.5	236.43
VSC1	SC	LW FSDT	394.6	33.21	179.3	54.17	140.8	90.86	124.2	207.76
		LW F/F/T/F/F	394.6	33.21	179.3	54.17	140.8	90.86	124.2	207.76
		LW F/T/T/T/F	394.6	33.21	179.2	54.15	140.4	90.77	122.5	206.91
	$G_p = 11$	LW FSDT	534.0	46.31[a]	169.5	118.53[b]	162.8	96.5	142.8	220.62
		LW F/F/T/F/F	534.0	46.31[a]	169.5	118.53[b]	162.8	96.5	142.8	220.62
		LW F/T/T/T/F	533.9	46.30[a]	169.1	118.43[b]	162.4	96.4	141.1	220.10
VSC2	SC	LW FSDT	420.7	33.37	207.8	57.30	123.5	232.04	114.2	186.99
		LW F/F/T/F/F	420.7	33.37	207.8	57.30	123.5	232.04	114.2	186.99
		LW F/T/T/T/F	420.7	33.37	207.7	57.29	117.6	231.43	113.3	186.88
	$G_p = 11$	LW FSDT	578.3	46.34[a]	249.6	61.23	75.1	230.7[c]	79.5	534.57[c]
		LW F/F/T/F/F	578.3	46.34[a]	249.6	61.23	75.1	230.7[c]	135.8	279.63[a]
		LW F/T/T/T/F	578.3	46.34[a]	249.5	61.23	67.6	230.1[c]	133.7	278.50[a]

[a] Flutter due to the third and fourth modes.
[b] Flutter due to the sixth and seventh modes.
[c] Flutter due to the seventh and eighth modes; otherwise due to the first two modes.

regarding the side-to-thickness ratio $a/h = 250$, and are very close for $a/h = 100$, with maximum discrepancy of 0.1% relative to the most refined model. Hence, it is concluded that the piecewise FSDT model ensures the most favourable trade-off between numerical accuracy and computational efficiency for supersonic flutter analysis of thin sandwich panels with soft purely elastic core.

As the side-to-thickness ratio decreases, the role of the transverse shear deformations in the aeroelastic response of the panels increases, such that the discrepancies between the different LW kinematic models appear more noticeable. For moderately thick panels with $a/h = 50$, the proposed LW models are in good agreement for the case of *CSC* and *VSC1* elastic layers, with relative discrepancies lower than 1%, but some major discrepancies can be perceived for the case of *VSC2* elastic layers. In the particular case of *VSC2* elastic layers, in SC conditions, the LW model that involves the FSDT for the elastic composite layers predicts the nondimensionalized flutter pressure parameter 5% higher than the LW model that makes use of the TSDT for both the elastic composite layers and viscoelastic core. Likewise, for active proportional control conditions, the corresponding discrepancies increase to 11%, which clearly highlights the need for refined high-order kinematic models to obtain accurate aeroelastic flutter estimations when considering moderately thick sandwich panels with soft core. Nonetheless, despite the significant discrepancies in terms of nondimensionalized flutter pressure parameters in this particular test case, the flutter frequencies predicted by the different models are in good agreement.

For moderately thick panels with $a/h = 20$, regardless of the fibres configurations and electrical conditions, the LW models that involve the FSDT for the elastic composite layers tend to predict sightly higher nondimensionalized flutter pressure parameters than the LW model that makes use of the TSDT for both the elastic composite layers and soft core (discrepancies between 1% to 2%). The only exception is indeed verified for the case of *VSC2* elastic layers and active proportional control conditions, where the nondimensionalized flutter pressure parameter predicted by the piecewise linear model is approximately 41% lower than the value estimated by the high-order models. It is worth noting that among all the test cases, this is the only one where the piecewise linear model estimates that flutter occurs in modes different from those identified by the high-order models. In contrast, the discrepancy in terms of nondimensionalized flutter pressure parameter of the LW model that assumes the TSDT for the core alone to the further refined LW model that involves the TSDT for both the elastic composite layers and soft core is merely 1.6%, which is a value similar to the one obtained in the

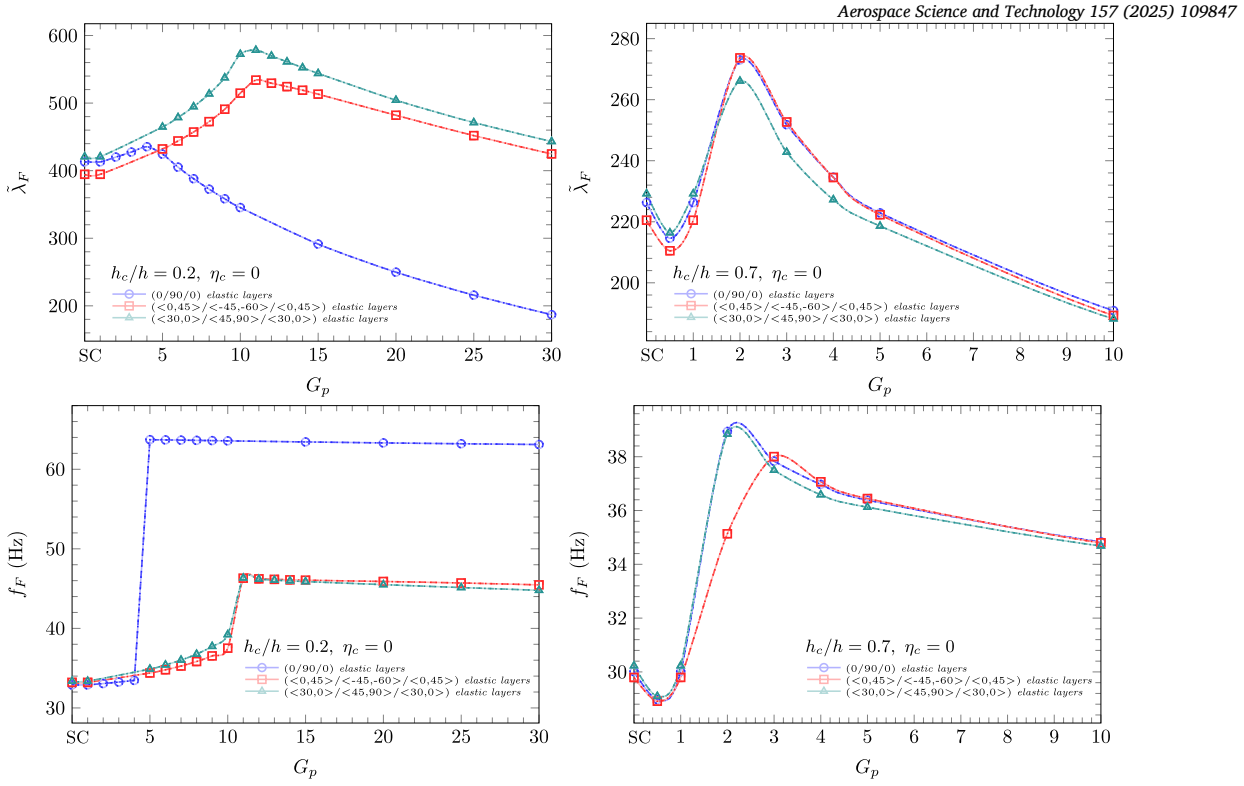

Fig. 3. Evolution of the nondimensionalized flutter pressure parameter $\tilde{\lambda}_F$ and flutter frequency f_F with the proportional feedback gain G_p of smart sandwich panels with purely elastic core ($a/h = 250$): LW FSDT (dotted lines), LW F/F/T/F/F (dashed lines) and LW F/T/T/T/F (solid lines) models.

remaining test cases of panels with $a/h = 20$. Even though the overall results suggest that for either thin or moderately thick plates there is no significant advantage of assuming the TSDT over the FSDT for the core alone, this specific outlier reveals that the accurate modelling of the transverse shear deformations and in-plane deformations within the core is *per se* relevant in the aeroelastic supersonic flutter analysis of moderately thick sandwich panels with soft core. It is also important to emphasize that the discrepancies relative to the most refined model tend to be higher when dealing with panels that experience flutter due to high-order modes since the transverse shear deformations are commonly more relevant in these modes as compared to the fundamental mode.

To provide further understanding on the impact of the proportional feedback gain on the aeroelastic response of smart sandwich panels with purely elastic core, Fig. 3 includes not only the case of a narrow core ($h_c/h = 0.2$) but also the case of a wide core ($h_c/h = 0.7$). As regards to the aeroelastic response of sandwich panels with a narrow viscoelastic core, the variable stiffness configurations greatly outperform the standard configuration of straight fibre composites for the vast majority of control gains. This is explained by the fact the sandwich panel with cross-ply composite layers exhibit flutter due to the sixth and seventh modes for control gain above the one that leads to the maximum flutter resistance. As shown by Moreira et al. [27], flutter due to the high-order modes, such as the sixth and seventh modes, is commonly related to the occurrence of natural frequencies that are very close to each other, which tend to coalesce for lower nondimensionalized pressure parameters than the first four modes. For the case of wide core, the fibres configurations of the elastic composite layers do not affect significantly the aeroelastic response since it is mostly dominated by the predominant soft core material. Hence, the maximum flutter resistance is achieved for the same proportional feedback gain, $G_p = 2$, regardless of the elastic layers. The previously mentioned control gain leads to relative increases of 21%, 24% and 16% for the *CSC*, *VSC1* and *VSC2* elastic layers, respectively, in relation to the nondimensionalized flutter pressure parameter of the corresponding uncontrolled system. As compared to the case of narrow core, the sandwich panels with wide purely elastic core require a lower control gain to achieve the maximum flutter resistance, while maintaining considerable improvements with respect to SC conditions.

The changes of the modes involved in the occurrence of flutter, from the first two modes to the high-order modes, are commonly associated with a pronounced jump in the flutter frequency value, as shown in Fig. 3. For sandwich panels with narrow core, flutter emerges due to the first two modes for SC conditions and active control conditions with proportional feedback gains up to the maximum flutter resistance. More specifically, for the case of VSC layers, the control gain that leads to the maximum flutter resistance ($G_p = 11$) marks the point where the panels start to experience flutter due to the third and fourth modes. However, for the cross-ply elastic layers, the maximum nondimensionalized flutter pressure parameter is achieved while flutter still occurs due to the coupling of the first two modes, which then changes for the sixth and seventh modes as the control gain increases. For sandwich panels with wide core, the modes that lead to the flutter instability also change from the first two modes, in the case of SC conditions, to the third and fourth modes as the proportional feedback gain increases. In fact, for the smart sandwich panels with *CSC* elastic layers and *VSC2* elastic layers, the value of control gain that yields the maximum flutter resistance is obtained when flutter stars to arise in the third and fourth modes, whereas for the case of *VSC1* elastic layers, the point of maximum flutter resistance remains associated to the coupling of the first two modes. Hence, it is concluded that for proportional feedback gains around the value that leads to the maximum flutter resistance, there is usually an alteration of the modes participating in flutter.

The advantageous effect of the proportional feedback gain on the aeroelastic response is further illustrated in Fig. 4 through the evolution of the natural frequencies and modal loss factors with the nondimensionalized pressure parameter. Since the aerodynamic and viscoelastic damping are neglected, the modal loss factors are null prior to the occurrence of flutter. As the natural frequencies coalesce to the same value, the corresponding modal loss factors arise as non zero symmetric val-

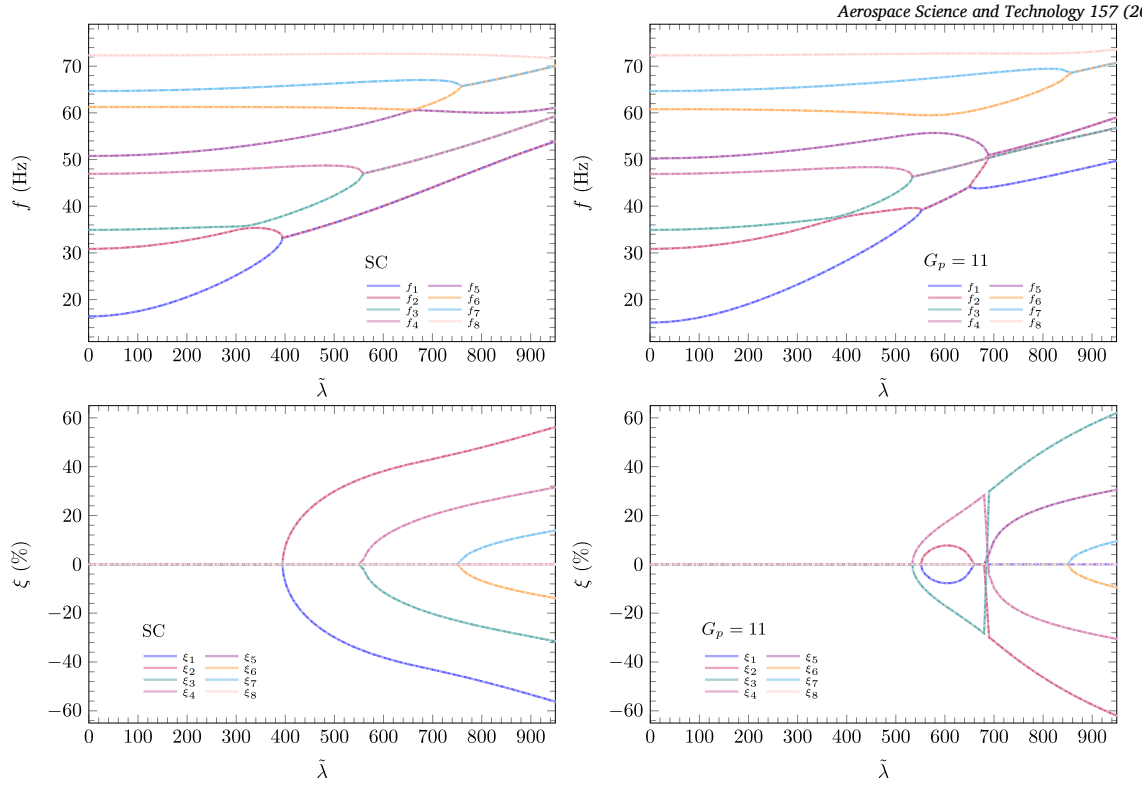

Fig. 4. Variation of the first eight natural frequencies f_n and modal loss factors ξ_n(%) with the nondimensionalized pressure parameter $\tilde{\lambda}$ of the smart sandwich panel with purely elastic core and *VSC1* elastic layers ($a/h = 250$, $h_c/h = 0.2$ and $\eta_c = 0$), under SC conditions or proportional feedback gain $G_p = 11$: LW FSDT (dotted lines), LW F/F/T/F/F (dashed lines) and LW F/T/T/T/F (solid lines) models.

ues, noting that the flutter bound is defined by the first occurrence of coupled modes.

Fig. 4 also shows that the proportional feedback gain postpones the coalescence of the first two modes, which are the ones responsible for the occurrence of flutter in SC conditions, such that flutter starts to arise due to the third and fourth modes. In fact, the frequencies and modal loss factors of the third and fourth modes remain mostly unchanged when the active proportional control is applied, whereas the coalescence of the sixth and seventh modes is delayed. Moreover, it is interesting to highlight that for active control conditions with proportional feedback gain $G_p = 11$, the first two modes couple slightly after the coalescence of the third and fourth modes, but decouple as the pressure parameter increases. After this point, the third and fourth modes also decouple, giving rise to the coalescence of the second and third modes as well as the fourth and fifth modes. From a structural modelling point of view, Fig. 4 emphasizes that the three LW models are in excellent agreement for the evaluation of the natural frequencies and modal loss factors of thin supersonic sandwich panels with purely elastic core.

Even though the proportional feedback control law affects positively the flutter resistance of the smart sandwich panels with purely elastic core, the derivative feedback control law shows the opposite effects in the present test cases, as also shown in a previous work by Song and Li [55] regarding smart composite laminates. Taking the case of sandwich panels with *VSC1* elastic layers ($a/h = 250$ and $h_c/h = 0.2$) as an example, and considering SC conditions as standpoint, the use of $G_d = 10^{-5}$ or $G_d = 10^{-4}$ leads to a reduction of 2% in the nondimensionalized flutter pressure parameter, whereas for $G_d = 10^{-3}$ and $G_d = 10^{-2}$ it is observed a reduction of 17% and 65%, respectively. These results are in agreement with the fact that structural damping can have either a stabilizing or destabilizing effect on the occurrence of couple-mode flutter [20], noting that in this case structural damping arises from the derivative feedback control law. In fact, the added active stiffness resulting from the proportional feedback control law is capable of altering the natural frequencies and their coupling behaviour, from which flutter emerges in the case of sandwich panels with purely elastic core, whereas the added active damping impacts mostly the loss factors.

5.3. Smart sandwich panels with viscoelastic core

Table 5 presents the assessment of the LW models for supersonic flutter analysis of smart viscoelastic sandwich panels with unidirectional or curvilinear fibre elastic layers. More precisely, the nondimensionalized flutter pressure parameters and the single mode involved in the occurrence of flutter are presented, considering both narrow and wide viscoelastic core, as well as thin and moderately thick plates. In addition, the results are provided considering both SC conditions of the surface electrodes and active derivative control conditions, noting that the derivative feedback gains G_d are selected to ensure the maximum flutter resistance when considering thin sandwich panels with $a/h = 250$. For brevity, the proportional feedback control law is not contemplated in the models accuracy assessment presented in Table 5 since the derivative feedback control law is the most advantageous and effective for active flutter control of viscoelastic sandwich panels, as explained later on.

In accordance with Fig. 5, for the case of narrow viscoelastic core, the maximum flutter resistance is achieved making use of $G_d = 0.075$ for the sandwich panels with *CSC* and *VSC1* elastic layers, and $G_d = 0.050$ for *VSC2* elastic layers. The previously mentioned control gains result in relative increases of 88%, 64% and 90% for the *CSC*, *VSC1*, and *VSC2* elastic layers, respectively, in relation to the nondimensionalized flutter pressure parameter of the corresponding uncontrolled system. Furthermore, for the case of wide core, the maximum nondimensionalized flutter pressure parameters are obtained for $G_d = 0.075$ regardless of the elastic composite layers. Considering the flutter bound of the uncontrolled systems, the sandwich panels with *CSC*, *VSC1*, and *VSC2* elastic layers experience maximum relative increases of 74%, 63%, and 71%, respectively.

Table 5
Nondimensionalized flutter pressure parameters $\tilde{\lambda}_F$ of smart viscoelastic sandwich panels with narrow ($h_c/h = 0.2$) or wide core ($h_c/h = 0.7$), considering unidirectional or curvilinear fibre elastic layers, under SC conditions or active derivative control G_d.

			$h_c/h = 0.2$				$h_c/h = 0.7$			
Case	E.C.	Model	$a/h = 250$	$a/h = 100$	$a/h = 50$	$a/h = 20$	$a/h = 250$	$a/h = 100$	$a/h = 50$	$a/h = 20$
CSC	SC	LW FSDT	226.0	165.0	147.1	137.8	96.9	29.4	12.0	7.09
		LW F/F/T/F/F	226.0	165.0	147.1	137.8	96.9	29.4	12.0	7.09
		LW F/T/T/T/F	226.0	164.9	146.7	135.6	96.9	29.4	12.0	7.08
	$G_d = 0.075$	LW FSDT	424.7[a]	180.0[b]	95.4[b]	41.7[b]	168.5[a]	36.1	14.0	5.66[b]
		LW F/F/T/F/F	424.7[a]	180.0[b]	95.4[b]	41.7[b]	168.5[a]	36.1	14.0	5.66[b]
		LW F/T/T/T/F	424.7[a]	179.8[b]	94.3[b]	38.2[b]	168.5[a]	36.1	14.0	5.64[b]
VSC1	SC	LW FSDT	238.7	142.2	119.2	108.2	104.7	29.2	11.8	6.88
		LW F/F/T/F/F	238.7	142.2	119.2	108.2	104.7	29.2	11.8	6.88
		LW F/T/T/T/F	238.6	142.1	118.8	106.5	104.6	29.2	11.8	6.87
	$G_d = 0.075$	LW FSDT	391.4[a]	160.6[a]	74.9[b]	26.6[b]	170.5[a]	35.5	13.8	4.98[b]
		LW F/F/T/F/F	391.4[a]	160.6[a]	74.9[b]	26.6[b]	170.5[a]	35.5	13.8	4.98[b]
		LW F/T/T/T/F	391.3[a]	160.5[a]	74.4[b]	25.2[b]	170.5[a]	35.5	13.8	4.97[b]
VSC2	SC	LW FSDT	224.0	150.0	110.6	87.5	97.0	29.5	11.8	5.77
		LW F/F/T/F/F	224.0	150.0	110.6	87.5	97.0	29.5	11.8	5.77
		LW F/T/T/T/F	224.0	150.0	110.5	86.6	97.0	29.5	11.8	5.76
	$G_d = 0.050$[c]	LW FSDT	425.2[a]	190.4[a]	110.1[b]	39.6[a]	165.8[a]	37.3	13.8	5.50[a]
		LW F/F/T/F/F	425.2[a]	190.4[a]	110.1[b]	39.6[a]	165.8[a]	37.3	13.8	5.50[a]
		LW F/T/T/T/F	425.2[a]	190.3[a]	109.4[b]	39.2[a]	165.8[a]	37.3	13.8	5.50[a]

[a] Flutter due to the second mode.
[b] Flutter due to the third mode; otherwise due to the first mode.
[c] $G_d = 0.075$ if $h_c/h = 0.7$.

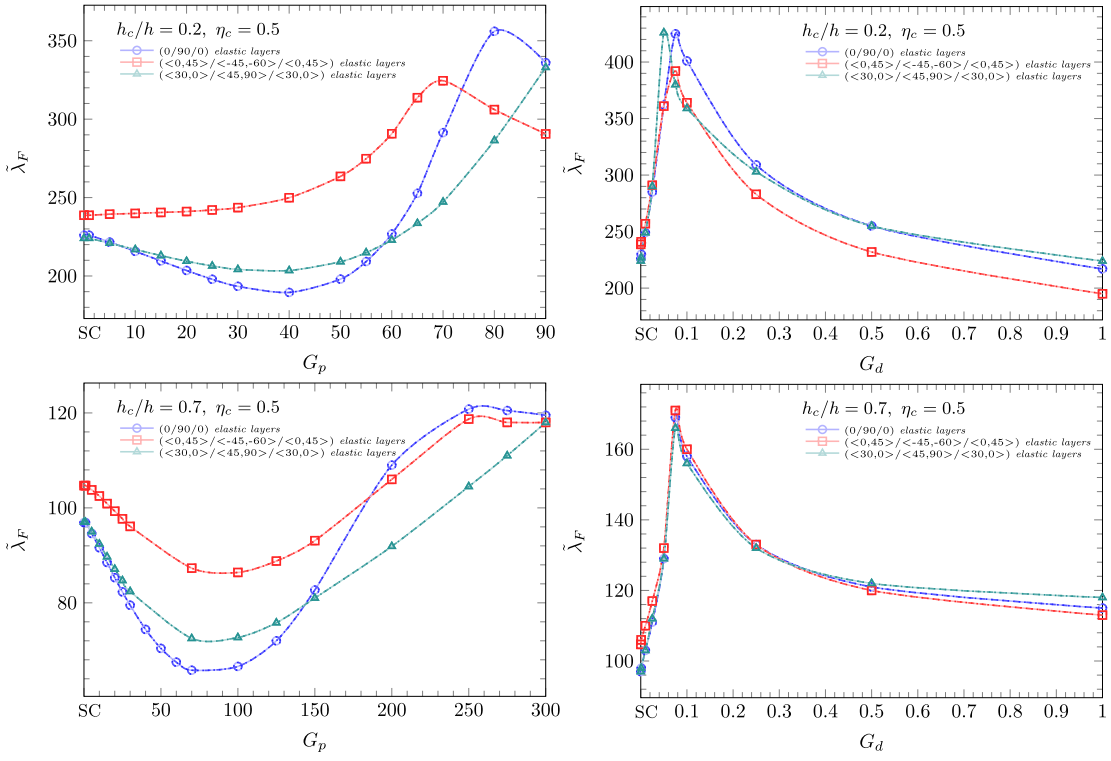

Fig. 5. Evolution of the nondimensionalized flutter pressure parameter $\tilde{\lambda}_F$ with the proportional and derivative feedback gains G_p and G_d - first and second columns, respectively - of smart viscoelastic sandwich panels ($a/h = 250$): LW FSDT (dotted lines), LW F/F/T/F/F (dashed lines) and LW F/T/T/T/F (solid lines) models.

As far as thin sandwich panels are concerned, the flutter bounds predicted by the three LW models are in very good agreement between each other, as also pointed out for the case of sandwich panels with purely elastic core. This is verified for both core thickness ratios, regardless of the elastic composite layers and control conditions. To be precise, the different kinematic models estimate similar nondimensionalized flutter pressure parameters even when dealing with moderately thick plates with $a/h = 50$. However, for moderately thick plates with $a/h = 20$ and narrow core $h_c/h = 0.2$, significant discrepancies arise between the LW models that make use of the FSDT for the elastic composite layers and the further refined LW model involving the TSDT for any non piezoelectric layer. These discrepancies range between 1% and 9%, being higher when the applied derivative feedback gain leads to the occurrence of flutter in the third mode (i.e. case of *CSC* and *VSC1* elastic layers) rather

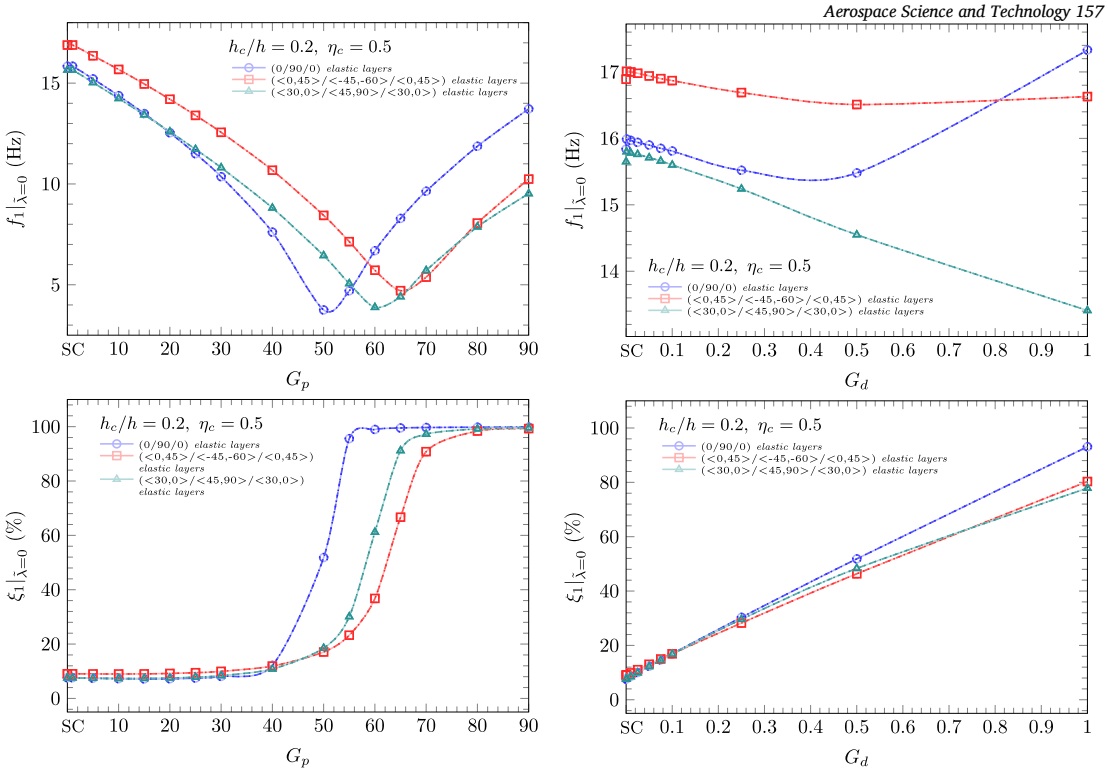

Fig. 6. Evolution of the fundamental frequency in vacuum $f_1|_{\tilde{\lambda}=0}$ and corresponding modal loss factor $\xi_1|_{\tilde{\lambda}=0}$ with the proportional and derivative feedback gains G_p and G_d - first and second columns, respectively - of smart viscoelastic sandwich panels ($a/h = 250$, $h_c/h = 0.2$): LW FSDT (dotted lines), LW F/F/T/F/F (dashed lines) and LW F/T/T/T/F (solid lines) models.

than when it arises due to the second mode (case of *VSC2* elastic layers) or the first mode (case of SC conditions).

In Table 5, the solutions for moderately thick plates with $a/h = 20$ and $h_c/h = 0.7$ are presented with increased precision since the nondimensionalized flutter pressure parameters are quite reduced ($\tilde{\lambda}_F < 10$) in comparison to the remaining test cases. Even so, the LW models predict very similar flutter solutions despite the reduced side-to-thickness ratio, as opposed to what is verified in the case of a narrow core. Actually, since the thickness ratio of the composite layers is very low in sandwich panels with wide core, resulting in a reduced contribution to the overall transverse shear deformation energy, the refinements introduced in the corresponding discrete layers by the TSDT over the FSDT render meaningless effects when the evaluation of the nondimensionalized flutter pressure parameter is concerned, even when considering moderately thick plates with $a/h = 50$ and 20.

Comparing the effect of the two control strategies on the variation of the nondimensionalized flutter pressure parameters, as shown in Fig. 5, it is evident that the derivative control promotes an immediate and sharp increase in flutter resistance, whereas the proportional control has a diminishing effect at lower control gain values, with exception of the sandwich panel with narrow core and *VSC1* elastic layers, which exhibits a smooth increasing trend. These tendencies are verified for smart sandwich panels with either narrow or wide viscoelastic core. Despite the non favourable impact of the proportional control in the lower range of control gains, this is reversed as the control gains continues to increase and flutter starts to arise due to the third mode instead of the first mode. In fact, for such aeroelastically favourable range of proportional feedback gains, Fig. 6 shows that the modal loss factor of the first mode in vacuum approaches $\xi_1 \approx 1$, i.e. $\xi_1(\%) \approx 100\%$.

The remarkable stabilizing impact of the derivative feedback control law in the presence of single mode flutter is further exemplified by the observation that, for a broad spectrum of derivative feedback gains exceeding the value that maximizes flutter resistance, the nondimensionalized flutter pressure parameters consistently surpass the corresponding values observed under SC conditions. It is worth emphasizing that as compared to sandwich panels with a narrow core, the panels with a wide core require even higher proportional feedback gains in order to achieve improvements in flutter resistance. However, when derivative control is considered, the range of beneficial control gains is quite similar for both core thickness ratios. This emphasizes further the superior authority and usefulness of the derivative feedback control law over the proportional feedback control law for effectively managing single mode flutter in viscoelastic sandwich panels.

To further understand the effect of the proportional and derivative feedback control laws on the dynamic and aeroelastic characteristics of the smart viscoelastic panels, Fig. 6 shows the evolution of the fundamental frequencies and corresponding modal loss factors in vacuum with the control gains. For low values of proportional feedback gain, the fundamental frequencies tend to decrease significantly and the modal loss factors remain almost constant, while the nondimensionalized flutter pressure parameter can be either decreasing or increasing very smoothly, as shown in Fig. 5. As the proportional feedback gain reaches a certain threshold value, the fundamental frequencies and corresponding modal loss factors start to increase, as well as the nondimensionalized flutter pressure parameter in Fig. 5. Note that by definition, the damped frequency, which corresponds to the imaginary part of the eigenvalues, approaches zero when the modal loss factor tends to $\xi_1 \approx 1$, which means that the motion will progressively loose its oscillatory behaviour. In this case, the eigenvalue emerges as a pure real number $s_1 = \omega_1 = 2\pi f_1$ and that is the reason for the increasing tendency of the natural frequencies as the modal loss factor approaches $\xi_1 \approx 1$.

Since the derivative feedback gain impacts mostly the damping characteristics rather than the actual stiffness of the panels, the fundamental frequencies are less influenced by the derivative feedback gain than by the proportional feedback gain (Fig. 6). Conversely, the derivative feedback control law has a more direct impact on the modal loss factor, as expected, and it is verified a quasi-linear relation between the funda-

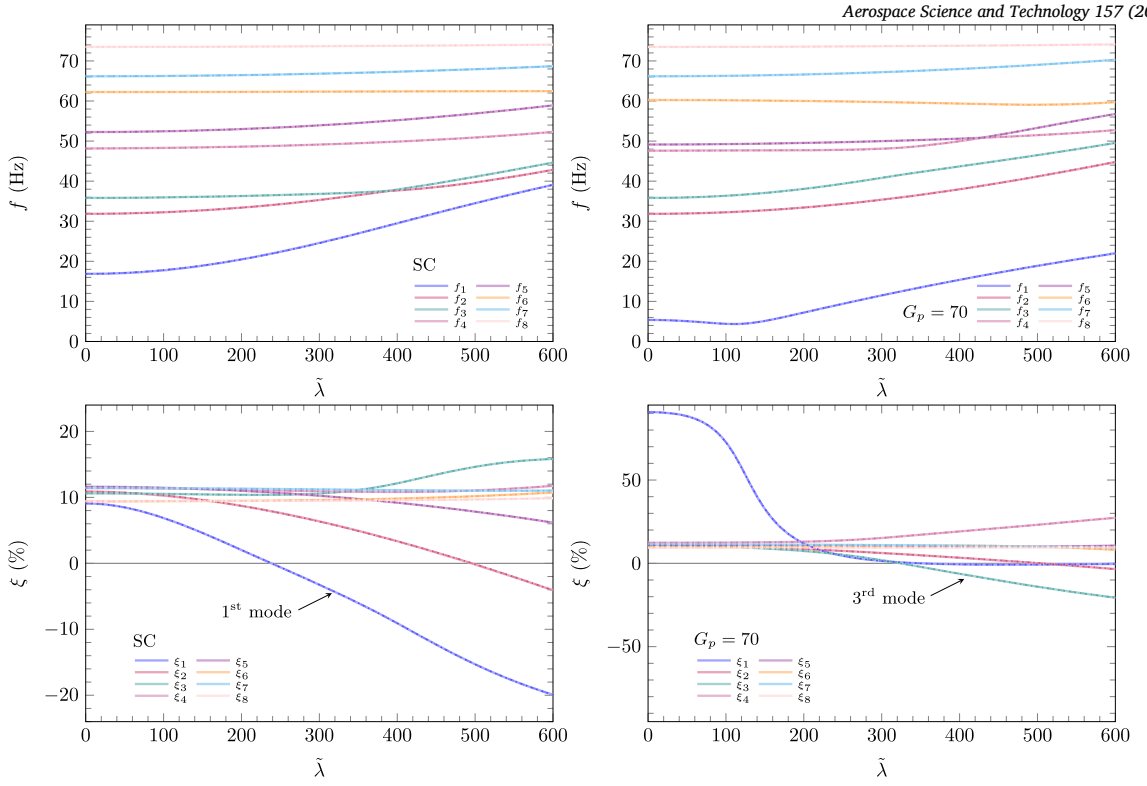

Fig. 7. Variation of the first eight natural frequencies f_n and modal loss factors $\xi_n(\%)$ with the nondimensionalized pressure parameter $\tilde{\lambda}$ of the smart viscoelastic sandwich panel with *VSC1* elastic layers ($a/h = 250$, $h_c/h = 0.2$), under SC conditions or proportional feedback gain $G_p = 70$: LW FSDT (dotted lines), LW F/F/T/F/F (dashed lines) and LW F/T/T/T/F (solid lines) models.

mental modal loss factor and the derivative feedback gain. At the same time, the derivative feedback gain can also be used to effectively enhance the nondimensionalized flutter pressure parameter (Fig. 5).

To illustrate the occurrence of flutter due to a single mode in viscoelastic sandwich panels under supersonic airflow, while providing a further understanding on the effect of the proportional and derivative feedback control laws on this type of flutter, the evolutions of the natural frequencies and modal loss factor with the nondimensionalized pressure parameter are provided in Figs. 7 and 8 for selected control states, considering thin panels, which are of primary interest for most aerospace applications. As shown in Fig. 7, for SC conditions, flutter occurs as the modal loss factor of the first mode moves from the positive half-plane (stable region) to the negative half-plane (unstable region). Even though there is a clear change in the sign of the first mode modal loss factor, there is no coalescence of natural frequencies nor pairs of symmetric modal loss factors, as opposed to the standard mechanism of coupled-mode flutter, previously shown for the case of sandwich panels with purely elastic core (Fig. 4). In fact, the structural damping tends to result on the non perfect coalescence of natural frequencies, i.e. the natural frequencies merely approach each other asymptotically [24,25,22]. Other than that, the occurrence of panel flutter due to a single mode has also been verified for low supersonic regimes, where the piston theory and other quasi-steady aerodynamic theories fail to predict this phenomenon since it arises as a result of the unsteady effects of the aerodynamic forces, as recently discussed by Ye et al. [63]. In the case of viscoelastic sandwich panels, the structural damping induced by the viscoelastic core affects all modes and is sufficiently high to dominate the aeroelastic behaviour, which turns out be aero-visco-elastic, promoting the complete decoupling of the modes, such that the progressive reduction of the modal loss factors plays a more significant role than the interactions between frequencies [20,21,23].

As detailed in Table 5, the occurrence of single mode flutter in viscoelastic sandwich panels is commonly related to the first mode, as also shown by Moreira et al. [27], but it can also arise in high-order modes when considering active control conditions. Regardless of the side-to-thickness ratio a/h and core thickness ratio h_c/h, smart viscoelastic sandwich panels experience flutter due to the first mode when engaged in SC conditions. In contrast, for active derivative control conditions, single mode flutter may arise among the first three modes depending on the side-to-thickness ratio, core thickness ratio and control gain. Specifically, Fig. 7 reveals that for thin panels with narrow viscoelastic core and proportional feedback gain $G_p = 70$, the third mode is the one that becomes aeroelastically unstable. However, for such high value of proportional feedback gain, the fundamental frequency is significantly reduced and the corresponding modal loss factor is close to $\xi_1 \approx 1$, i.e. $\xi_1(\%) \approx 100\%$, which means an overdamped mode, for low values of nondimensionalized pressure parameter. As the nondimensionalized pressure parameter increases, the fundamental frequency increases and the modal loss factor decreases until the point where it tangentially reaches $\xi_1 = 0$. To be precise, the modal loss factor of the fundamental mode becomes negative just slightly after the modal loss factor of the third mode.

When considering active derivative control conditions, Fig. 8 shows that flutter arises due to the second mode for the control gain that leads to the maximum flutter resistance ($G_d = 0.075$). To be precise, it is observed that the first mode is stabilized around the flutter bound, whereas the change of the sign of the modal loss factor associated to the second mode is anticipated as compared to SC conditions. Increasing the derivative feedback gain to $G_d = 0.250$, a careful examination of Figs. 7 and 8 reveals that the first mode is even further stabilized and the modal loss factor of the second mode remains mostly unchanged with respect to the case of SC conditions. In fact, flutter emerges due to the third mode and the nondimensionalized flutter pressure parameter is higher than for SC conditions, but clearly below the one obtained with $G_d = 0.075$. For both derivative feedback gains investigated in Fig. 8, it is interesting to note that there is a clear approximation of the natural frequencies in the vicinity of the flutter bound, which is especially noticeable in the second and third modes when applying $G_d = 0.250$. For $G_d = 0.075$, the first

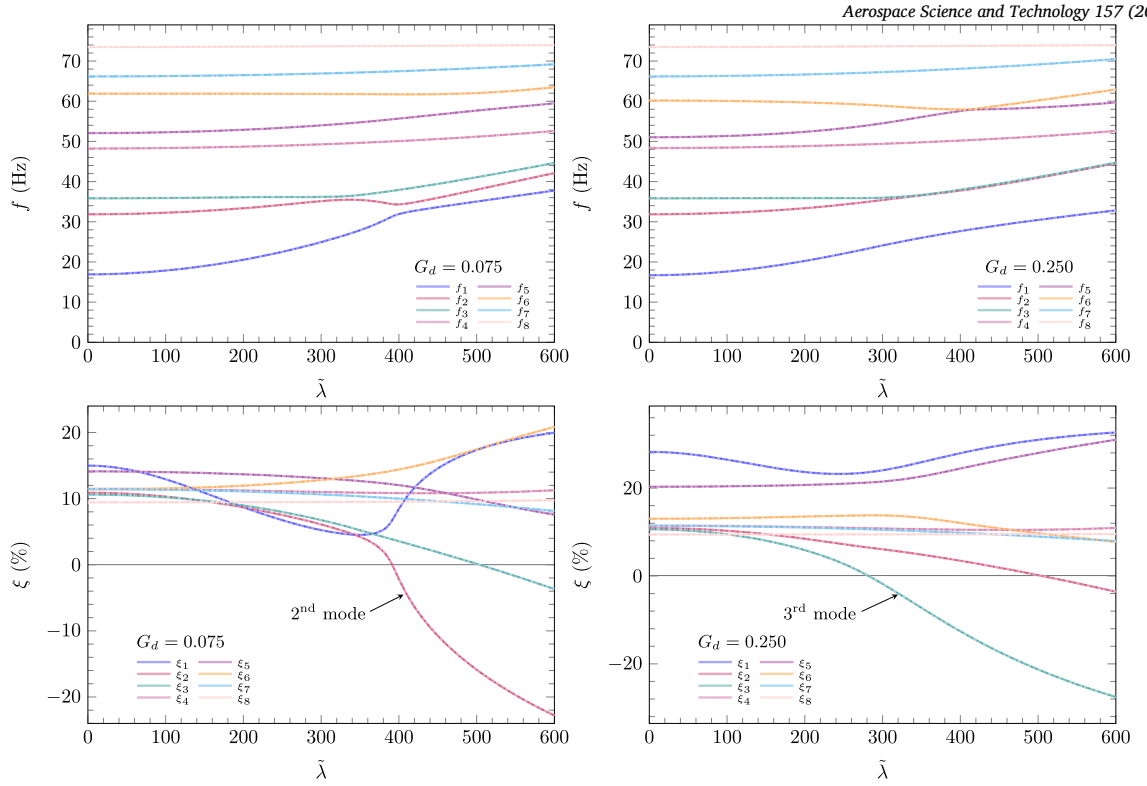

Fig. 8. Variation of the first eight natural frequencies f_n and modal loss factors ξ_n(%) with the nondimensionalized pressure parameter $\tilde{\lambda}$ of the smart viscoelastic sandwich panel with *VSC1* elastic layers ($a/h = 250$, $h_c/h = 0.2$), under derivative feedback gain $G_d = 0.075$ and 0.250: LW FSDT (dotted lines), LW F/F/T/F/F (dashed lines) and LW F/T/T/T/F (solid lines) models.

two natural frequencies approach each other around the flutter bound, but they get far apart as the nondimensionalized pressure parameter increases because flutter arises merely due to the second mode, without any coalescence of natural frequencies, as expected in viscoelastic sandwich panels with properties described through the complex modulus approach [20,27].

To be precise, for the range of derivative feedback gains explored in Fig. 5, three successive phases of single mode flutter are observed in all test cases, regardless of the core thickness ratio. As the derivative feedback gain increases, the mode that leads to flutter changes progressively from the first mode, as in SC conditions, to the second mode, and then to the third mode, noting that the maximum flutter resistance tends to be related to the occurrence of instability in the second mode. Nevertheless, the precise range of derivative feedback gains associated to each phase depends not only on the core thickness ratio but also on the fibre distributions of the elastic composite layers.

Comparing the proportional and derivative feedback control laws, it can be pointed out that the derivative feedback gain can stabilize the occurrence of flutter due to the first mode in a more effective fashion, such that flutter ends up occurring in the high-order modes for superior values of nondimensionalized pressure parameter, while avoiding a significant reduction of the fundamental frequency. This conclusion contrasts to what is observed in sandwich panels with purely elastic core, where flutter occurs as the modes coalesce. In more detail, these distinct behaviours may be explained by the nature of the flutter instability and how can the control law affect the stiffness and damping characteristics of the panels. On one hand, the flutter phenomenon that results from the coalescence of modes is highly dominated by the evolution and interaction of the natural frequencies and, therefore, the active stiffness added by the proportional feedback gain can be useful to tailor the natural frequencies and reshape the interaction between modes, while the derivative control tackles primarily the modal loss factors. On the other hand, the occurrence of flutter due to a single mode is driven exclusively by the trends of the modal loss factors (Figs. 7 and 8), which can be easily adjusted by the active damping resulting from the derivative control law rather than by the active stiffness induced through proportional control, recalling that the modal loss factor in vacuum of the first mode increases merely for high values of proportional feedback gain, as shown in Fig. 6.

It is also worth mentioning that Figs. 3, 5 and 6 reveal different dynamic and aeroelastic responses, as well as distinct sensitivity levels to the control gains, depending on various design parameters, such as the fibre configurations of the elastic composite layers, the core thickness ratio and the viscoelastic core loss factor. Concerning smart sandwich panels with purely elastic core ($\eta_c = 0$), it is perceived from Fig. 3 that the *VSC2* elastic layers offer the maximum flutter resistance in the case of narrow core, regardless of the control conditions, but they are outperformed by the remaining fibre distributions in the case of wide core, even though the *VSC2* elastic layers still provide the higher flutter bound in SC conditions.

As regards to smart viscoelastic sandwich panels with a core loss factor $\eta_c = 0.5$, the configuration with *VSC1* elastic layers takes the lead in SC conditions, for both core thickness ratios (Fig. 5). More precisely, in SC conditions, the viscoelastic sandwich panels with *VSC1* elastic layers exhibit flutter bounds that are roughly 8% higher than those observed for the other elastic layers. When active proportional control is applied, the *VSC1* elastic layers also show higher nondimensionalized flutter pressure parameters at low proportional feedback gain values, but they end up outperformed by the other composite laminates as the gain increases. On the other hand, when considering derivative control, the impact of the elastic layers is mostly noticed in sandwich panels with narrow core ($h_c/h = 0.2$). Despite the fact that all composite laminates show similar trends for sandwich panels with wide core ($h_c/h = 0.7$), it is perceived that the *VSC1* elastic layers present slightly improved flutter bounds within the range of derivative feedback gains around the maximum flutter resistance. In the scenario of a narrow core, however, it is noted that the sandwich panels with *CSC* and *VSC2* elastic layers exhibit nearly identical maximum nondimensionalized flutter pressure param-

eters, exceeding the highest value achieved with *VSC1* elastic layers by approximately 9% (see Table 5 for the detailed numerical results).

From the point of view of the fundamental mode in vacuum, Fig. 6 shows that for viscoelastic sandwich panels with narrow core, the configuration with *VSC1* elastic layers also leads to the highest fundamental frequency for most of the proportional and derivative feedback gains. In contrast, the fundamental loss factor of the viscoelastic sandwich panel with *VSC1* elastic layers is surpassed by the remaining fibre distributions as the control gains increase.

In line with studies on panel flutter [20,21], the types of damping proportional to the velocity, such as the aerodynamic damping, have a stabilizing effect on the coupled-mode flutter, whereas the material damping proportional to both mass and stiffness and the viscoelastic complex modulus damping can be either stabilizing or destabilizing on this type of flutter, though the latter is more commonly observed [22,27]. This somewhat unexpected phenomenon of damping leading to instability is verified in the present work by noting that when considering SC conditions or active proportional control, for instance, the nondimensionalized flutter pressure parameters of the viscoelastic sandwich panels are significantly reduced as compared to the counterparts with purely elastic core (see Tables 4 and 5 as well as Figs. 3 and 5).

Although in the present numerical applications it is considered either $\eta_c = 0$ or $\eta_c = 0.5$, i.e. only one non zero value of core loss factor is investigated, a prior work by the authors [27] reveals that enhancements of the nondimensionalized flutter pressure parameters are attainable by increasing the core loss factor. As discussed in detail by Moreira et al. [27], for high values of core loss factor, the flutter bounds of the viscoelastic sandwich panels can even surpass the case of purely elastic core, depending on the type of elastic layers, core thickness ratio and boundary conditions, thus suggesting that viscoelastic damping is indeed suitable for the aeroelastic stability augmentation in supersonic sandwich panels.

In fact, when single mode flutter occurs, the damping terms have a stabilizing effect, i.e. by increasing the structural damping or the aerodynamic damping, the nondimensionalized flutter pressure parameters also increase [20]. To be precise, this effect is demonstrated in Fig. 5, when dealing with the derivative feedback control law, which provides active structural damping to the aeroelastic equilibrium equations of the panels. In addition, it is worth mentioning that the stabilizing effect of the active damping can postpone the occurrence of single mode flutter in smart viscoelastic sandwich panels for values of nondimensionalized pressure parameter near the coupled-mode flutter bound of the corresponding counterparts with purely elastic core under SC conditions. Moreover, in a more realistic scenario of non-linear viscoelastic materials with frequency- and temperature-dependent material properties, for which the flutter resistance may end up decreased due to the softening of the core or loss of its dissipative properties, it is expected that a proper selection of the proportional and derivative feedback gains can compensate the losses in stiffness and damping, respectively, at least in part. Hence, it is worth emphasizing that one of the limitations of the proposed models is the assumption of linear viscoelastic materials with frequency- and temperature-independent material properties, as well as the non-inclusion of geometrically non-linear effects. Additionally, the present models do not account for transverse normal stresses since it is considered shear deformation plate theories devoid of thickness stretching, which make use of plane stress constitutive equations. Nonetheless, the thickness stretching effects can be indeed neglected in the preliminary flutter analysis of supersonic viscoelastic sandwich panels [27]. Regarding the aerodynamic formulation, the present models involving the quasi-steady First-order Piston Theory are limited to the high supersonic regime, specifically within the range of $\sqrt{2} < M_\infty < 5$ [24,64], and the boundary layer effects are neglected since the aerodynamic theory considers inviscid linear flows [20].

To further explore and discuss the occurrence of single mode flutter in viscoelastic sandwich panels, Fig. 9 presents the evolution of the first two mode shapes for increasing values of nondimensionalized pressure parameter, taking as an example the smart viscoelastic sandwich panel with *VSC1* elastic layers and narrow core, under SC conditions. Since the eigenvalues and eigenvectors are complex, it is included both the real and imaginary parts of the in-plane mode shapes $w_0(x, y) = w(x, y, z = 0)$, i.e. $\Re(w_0)$ and $\Im(w_0)$, respectively, in addition to the absolute value $\sqrt{\Re(w_0)^2 + \Im(w_0)^2}$. Note that in this test case, flutter arises due to the first mode (Fig. 7).

As the nondimensionalized flutter pressure parameter increases, the aerodynamic loading deviates the modes in the direction of the airflow, which is the x-axis. It should be noted that upon reaching the flutter bound, the mode shapes of the first mode differ significantly from those of the second mode. Therefore, the occurrence of single mode flutter is verified beyond the natural frequencies and modal loss factors, shown in Fig. 7, since it is evident that the mode shapes do not merge into a single one.

All in all, it is concluded that the design optimization of the viscoelastic damping treatment and active piezoelectric layers or patches, along with the careful tailoring of the fibre angle distributions, are crucial for the successful development of cutting-edge aerospace technology involving lightweight and high-strength smart sandwich structures with improved aeroelastic flutter stability. For such purpose, it should be emphasized that the consistent agreement between the LW models shown in Table 5 and in Figs. 5 to 8 highlights the piecewise FSDT model as the most suitable structural model for active flutter control analyses and aero-visco-elastic design optimization works, concerning thin panels, since it ensures the same numerical accuracy as the high-order LW models, while requiring fewer DOF and a reduced computational effort.

6. Conclusions

The active aero-visco-elastic flutter control of supersonic smart sandwich panels combining viscoelastic materials along with variable stiffness composites and surface bonded piezoelectric sensor/actuator layers is investigated in this work, exploring variable-order LW models based on shear deformation theories, progressively refined to render numerically accurate and computationally efficient flutter predictions. In fact, this is the first work where first- and high-order LW kinematic descriptions are assessed for supersonic flutter analysis and active control in smart viscoelastic sandwich panels, while making a pioneering progress on the combined application of the emerging and highly promising variable stiffness composite (VSC) laminates, featuring curvilinear fibre distributions, with viscoelastic damping treatments and active piezoelectric materials for aeroelastic control.

An accuracy assessment of the proposed LW models is presented through selected numerical applications of smart sandwich panels, including either viscoelastic or purely elastic core, along with elastic layers made of composite laminates, using unidirectional or curvilinear fibres. Furthermore, the numerical applications are focused on simply supported panels under airflow aligned with the x-axis, encompassing both thin and moderately thick sandwich panels, with either narrow or wide core. From the structural modelling point of view, the models accuracy assessment in active flutter control analysis reveals that despite the fact that the LW FSDT model ensures a fair compromise between numerical accuracy and computational efficiency when considering thin sandwich panels, high-order models are of paramount importance for the proper aero-electro-visco-elastic modelling of moderately thick sandwich panels, especially when flutter arises due to high-order modes.

As regards to the adopted control laws, it is concluded that the proportional control has a notable stabilizing effect on the occurrence of coupled-mode flutter, as in smart sandwich panels with purely elastic core, whereas the derivative control demonstrates the opposite effect. Actually, it is observed that for the proportional feedback gain that leads to the maximum flutter resistance, or values close to it, there is an alteration of the modes involved in the occurrence of flutter as compared to the uncontrolled configuration. However, when dealing with smart viscoelastic sandwich panels, flutter arises due to a single mode, i.e.

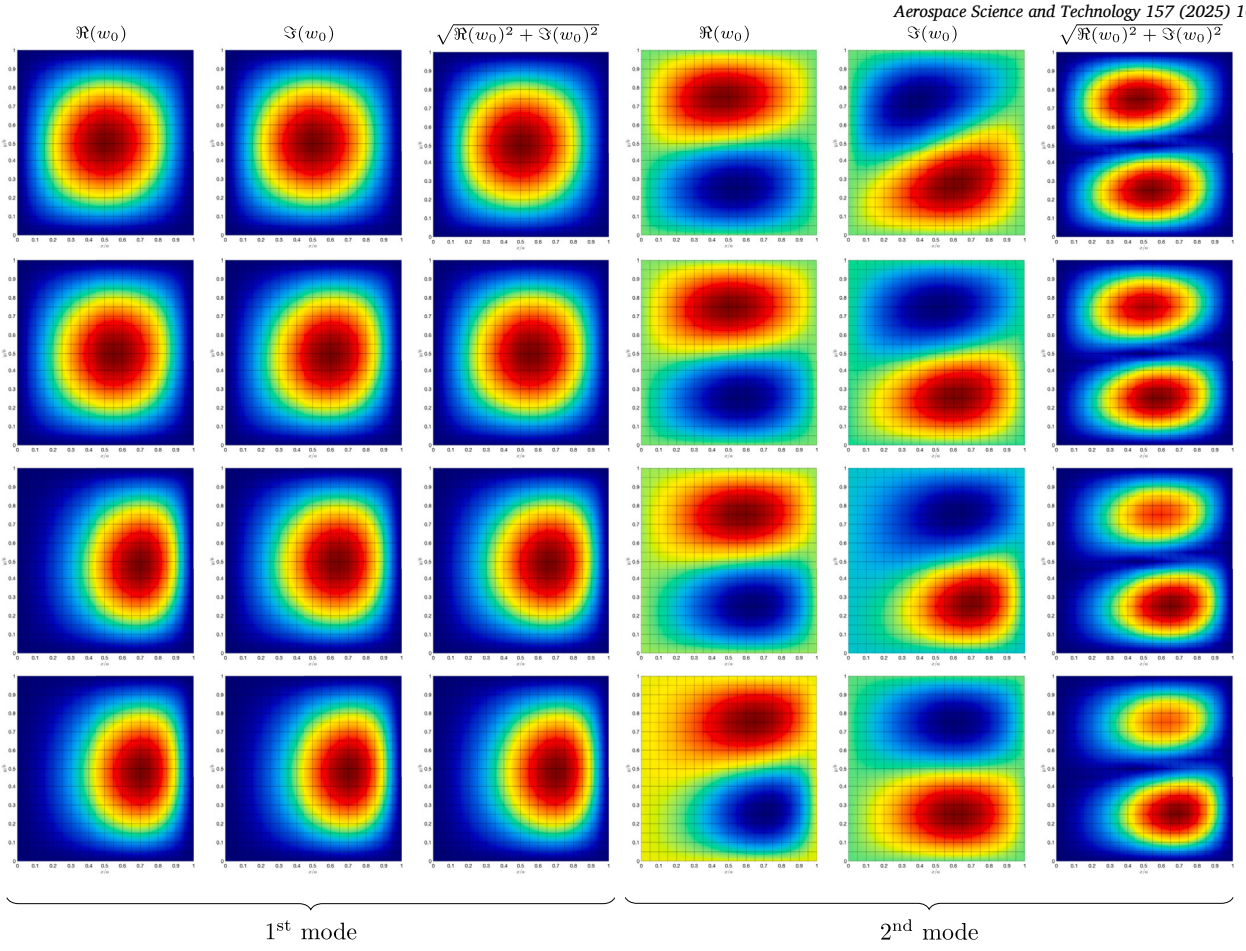

Fig. 9. First two in-plane mode shapes $w(x, y, 0)$ of the smart viscoelastic sandwich panel with *VSC1* elastic layers ($a/h = 250$, $h_c/h = 0.2$), in SC conditions, predicted by the LW FSDT model: $\tilde{\lambda} = 0$ in the first row, $\tilde{\lambda} = 0.25\tilde{\lambda}_F$ in the second row, $\tilde{\lambda} = 0.75\tilde{\lambda}_F$ in the third row and $\tilde{\lambda} = \tilde{\lambda}_F$ in the fourth row.

without coalescence of the modes, as a consequence of the complex modulus approach used to describe the behaviour of the viscoelastic core, thus resulting in distinct performances of the feedback control law as compared to the previously mentioned and most commonly found case of couple-mode flutter. On one hand, even though the proportional control can increase the flutter pressure parameters of viscoelastic sandwich panels, such positive impact is only verified for high values of proportional feedback gain. On the other hand, the derivative feedback control law demonstrates a more consistent stabilizing impact since it directly tackles the actual damping behaviour of the viscoelastic sandwich panels, playing a major role on the occurrence of aero-visco-elastic single mode flutter. In fact, the derivative feedback gain can effectively stabilize the first mode, which is responsible for flutter when the uncontrolled configurations are considered, such that flutter starts to arise in the second or third modes at up to 90% higher values of nondimensionalized pressure parameter. Hence, it is pointed out that the derivative control is more effective than the proportional control for postponing the occurrence of single mode flutter in sandwich panels with viscoelastic core, thus providing a superior capability for improving the aero-visco-elastic response.

Overall, this work provides new and complete benchmarks for ensuing research on the active control and aero-visco-elastic flutter analysis of supersonic smart sandwich panels, which may address later on the multi-objective aeroelastic design optimization of curvilinear fibre composite laminates, viscoelastic damping treatments and active piezoelectric sensors and actuators, all together, to ensure the development of advanced smart composite structures featuring enhanced dynamic and aeroelastic characteristics. Investigations on the non-linear post flutter regime should also be carried out in future works, particularly in terms of stress analysis for fatigue and failure estimations. Ultimately, it is essential to highlight the exploration of more realistic viscoelastic models and different types of control strategies, as a rather relevant aspect to consider in the context of active aero-visco-elastic control.

CRediT authorship contribution statement

J.A. Moreira: Writing – review & editing, Writing – original draft, Visualization, Validation, Software, Resources, Project administration, Methodology, Investigation, Funding acquisition, Formal analysis, Data curation, Conceptualization. **F. Moleiro:** Writing – review & editing, Supervision, Project administration, Methodology, Funding acquisition, Conceptualization. **A.L. Araújo:** Writing – review & editing, Supervision, Methodology, Funding acquisition, Conceptualization. **A. Pagani:** Writing – review & editing, Supervision, Funding acquisition, Conceptualization.

Declaration of competing interest

The authors declare that they have no known competing financial interests or personal relationships that could have appeared to influence the work reported in this paper.

Acknowledgements

The authors acknowledge Fundação para a Ciência e a Tecnologia (FCT) for its financial support via the project LAETA Base Funding UIDB/50022/2020 (DOI: 10.54499/UIDB/50022/2020). In addition, J.A. Moreira appreciates the financial support of Fundação para

a Ciência e a Tecnologia through the PhD Grant 2021.06113.BD (DOI: 10.54499/2021.06113.BD). A. Pagani acknowledges funding from the European Research Council (ERC) under the European Union's Horizon 2020 research and innovation programme (Grant agreement No. 850437).

Data availability

The data that supports the findings of this study is available from the corresponding author upon reasonable request.

References

[1] A. Racionero Sánchez-Majano, A. Pagani, Buckling and fundamental frequency optimization of tow-steered composites using layerwise structural models, AIAA J. 61 (9) (2023) 4149–4163, https://doi.org/10.2514/1.J062976.

[2] A. Pagani, A. Racionero Sánchez-Majano, D. Zamani, M. Petrolo, E. Carrera, Fundamental frequency layer-wise optimization of tow-steered composites considering gaps and overlaps, Aerotec. Missili Spaz. (2024), https://doi.org/10.1007/s42496-024-00212-w.

[3] O. Stodieck, J.E. Cooper, P.M. Weaver, P. Kealy, Improved aeroelastic tailoring using tow-steered composites, Compos. Struct. 106 (2013) 703–715, https://doi.org/10.1016/j.compstruct.2013.07.023.

[4] T.A. Guimarães, S.G. Castro, C.E. Cesnik, D.A. Rade, Supersonic flutter and buckling optimization of tow-steered composite plates, AIAA J. 57 (1) (2019) 397–407, https://doi.org/10.2514/1.J057282.

[5] P. Shivashankar, S. Gopalakrishnan, Review on the use of piezoelectric materials for active vibration, noise and flow control, Smart Mater. Struct. 29 (5) (2020) 053001, https://doi.org/10.1088/1361-665x/ab7541.

[6] A.L. Araújo, J.F.A. Madeira, Multiobjective optimization solutions for noise reduction in composite sandwich panels using active control, Compos. Struct. 247 (2020) 112440, https://doi.org/10.1016/j.compstruct.2020.112440.

[7] S. Raja, A.A. Pashilkar, R. Sreedeep, J.V. Kamesh, Flutter control of a composite plate with piezoelectric multilayered actuators, Aerosp. Sci. Technol. 10 (5) (2006) 435–441, https://doi.org/10.1016/j.ast.2006.01.003.

[8] N. Tsushima, W. Su, Flutter suppression for highly flexible wings using passive and active piezoelectric effects, Aerosp. Sci. Technol. 65 (2017) 78–89, https://doi.org/10.1016/j.ast.2017.02.013.

[9] H. Liu, X. Wang, Aeroservoelastic design of piezo-composite wings for gust load alleviation, J. Fluids Struct. 88 (2019) 83–99, https://doi.org/10.1016/j.jfluidstructs.2019.04.010.

[10] V.M. Kuriakose, V.M. Sreehari, Study on passive flutter control of damaged composite laminates with piezoelectric patches employing finite element method, Compos. Struct. 269 (2021) 114021, https://doi.org/10.1016/j.compstruct.2021.114021.

[11] S.H. Moon, J.S. Hwang, Panel flutter suppression with an optimal controller based on the nonlinear model using piezoelectric materials, Compos. Struct. 68 (3) (2005) 371–379, https://doi.org/10.1016/j.compstruct.2004.04.002.

[12] S.M. Hasheminejad, M. Aghayi Motaaleghi, Aeroelastic analysis and active flutter suppression of an electro-rheological sandwich cylindrical panel under yawed supersonic flow, Aerosp. Sci. Technol. 42 (2015) 118–127, https://doi.org/10.1016/j.ast.2015.01.004.

[13] M.V. Donadon, A.R. Faria, Aeroelastic behavior of composite laminated shells with embedded SMA wires under supersonic flow, Aerosp. Sci. Technol. 52 (2016) 157–166, https://doi.org/10.1016/j.ast.2016.02.026.

[14] Z.G. Song, F.M. Li, E. Carrera, P. Hagedorn, A new method of smart and optimal flutter control for composite laminated panels in supersonic airflow under thermal effects, J. Sound Vib. 414 (2018) 218–232, https://doi.org/10.1016/j.jsv.2017.11.008.

[15] H. Lin, C. Shao, D. Cao, Nonlinear flutter and random response of composite panel embedded in shape memory alloy in thermal-aero-acoustic coupled field, Aerosp. Sci. Technol. 100 (2020) 105785, https://doi.org/10.1016/j.ast.2020.105785.

[16] J. Wang, L. Zhou, L. Chen, M. Song, J. Yang, S. Kitipornchai, Aeroelastic flutter of actively controlled nanocomposite beams with an open edge crack, Aerosp. Sci. Technol. 141 (2023) 108498, https://doi.org/10.1016/j.ast.2023.108498.

[17] G.L. Ghiringhelli, M. Terraneo, E. Vigoni, Improvement of structures vibroacoustics by widespread embodiment of viscoelastic materials, Aerosp. Sci. Technol. 28 (1) (2013) 227–241, https://doi.org/10.1016/j.ast.2012.11.003.

[18] P.C.O. Martins, A.S. De Paula, S.H.S. Carneiro, D.A. Rade, Hybrid control technique applied to an aero-servo-viscoelastic simplified wing model, Aerosp. Sci. Technol. 122 (2022) 107387, https://doi.org/10.1016/j.ast.2022.107387.

[19] M.H. Hajmohammad, A. Farrokhian, R. Kolahchi, Smart control and vibration of viscoelastic actuator-multiphase nanocomposite conical shells-sensor considering hygrothermal load based on layerwise theory, Aerosp. Sci. Technol. 78 (2018) 260–270, https://doi.org/10.1016/j.ast.2018.04.030.

[20] E.H. Dowell, Panel flutter - a review of the aeroelastic stability of plates and shells, AIAA J. 8 (3) (1970) 385–399, https://doi.org/10.2514/3.5680.

[21] K.-N. Koo, W.-S. Hwang, Effects of hysteretic and aerodynamic damping on supersonic panel flutter of composite plates, J. Sound Vib. 273 (3) (2004) 569–583, https://doi.org/10.1016/S0022-460X(03)00514-5.

[22] H. Akhavan, P. Ribeiro, Aeroelasticity of composite plates with curvilinear fibres in supersonic flow, Compos. Struct. 194 (2018) 335–344, https://doi.org/10.1016/j.compstruct.2018.03.101.

[23] A.G. Cunha-Filho, A.M.G. de Lima, M.V. Donadon, L.S. Leão, Flutter suppression of plates subjected to supersonic flow using passive constrained viscoelastic layers and Golla–Hughes–McTavish method, Aerosp. Sci. Technol. 52 (2016) 70–80, https://doi.org/10.1016/j.ast.2016.02.022.

[24] X.-D. Yang, T.-J. Yu, W. Zhang, Y.J. Qian, M.H. Yao, Damping effect on supersonic panel flutter of composite plate with viscoelastic mid-layer, Compos. Struct. 137 (2016) 105–113, https://doi.org/10.1016/j.compstruct.2015.11.020.

[25] S. Mahmoudkhani, M. Sadeghmanesh, H. Haddadpour, Aero-thermo-elastic stability analysis of sandwich viscoelastic cylindrical shells in supersonic airflow, Compos. Struct. 147 (2016) 185–196, https://doi.org/10.1016/j.compstruct.2016.03.020.

[26] M. Mokhtari, M.R. Permoon, H. Haddadpour, Aeroelastic analysis of sandwich cylinder with fractional viscoelastic core described by Zener model, J. Fluids Struct. 85 (2019) 1–16, https://doi.org/10.1016/j.jfluidstructs.2018.11.013.

[27] J.A. Moreira, F. Moleiro, A.L. Araújo, A. Pagani, Layerwise models for supersonic flutter analysis of viscoelastic sandwich panels with curvilinear fibre composite skins, J. Sound Vib. 572 (2024) 118182, https://doi.org/10.1016/j.jsv.2023.118182.

[28] Y. Chai, W. Gao, B. Ankay, F.M. Li, C. Zhang, Aeroelastic analysis and flutter control of wings and panels: a review, Int. J. Mech. Syst. Dyn. 1 (1) (2021) 5–34, https://doi.org/10.1002/msd2.12015.

[29] J.N. Reddy, Mechanics of Laminated Composite Plates and Shells – Theory and Analysis, 2nd edition, CRC Press, Boca Raton, 2004.

[30] T.S. Plagianakos, E.G. Papadopoulos, Higher-order 2-D/3-D layerwise mechanics and finite elements for composite and sandwich composite plates with piezoelectric layers, Aerosp. Sci. Technol. 40 (2015) 150–163, https://doi.org/10.1016/j.ast.2014.10.015.

[31] K.M. Liew, Z.Z. Pan, L.W. Zhang, An overview of layerwise theories for composite laminates and structures: development, numerical implementation and application, Compos. Struct. 216 (2019) 240–259, https://doi.org/10.1016/j.compstruct.2019.02.074.

[32] H. Boudaoud, E.M. Belouettar, S. Daya, M. Potier-Ferry, A shell finite element for active-passive vibration control of composite structures with piezoelectric and viscoelastic layers, Mech. Adv. Mat. Struct. 15 (3–4) (2008) 208–219, https://doi.org/10.1080/15376490801907699.

[33] J.S. Moita, A.L. Araújo, V.M. Martins, P.G. Franco Correia, C.M. Mota Soares, C.A. Mota Soares, Analysis of active-passive plate structures using a simple and efficient finite element model, Mech. Adv. Mat. Struct. 18 (2) (2011) 159–169, https://doi.org/10.1080/15376494.2010.496062.

[34] A.L. Araújo, C.M. Mota Soares, C.A. Mota Soares, Finite element model for hybrid active-passive damping analysis of anisotropic laminated sandwich structures, J. Sandw. Struct. Mater. 12 (2010) 397–419, https://doi.org/10.1177/1099636209104534.

[35] A.L. Araújo, V.S. Carvalho, C.M. Mota Soares, J. Belinha, A.J.M. Ferreira, Vibration analysis of laminated soft core sandwich plates with piezoelectric sensors and actuators, Compos. Struct. 151 (2016) 91–98, https://doi.org/10.1016/j.compstruct.2016.03.013.

[36] Q. Wu, S. Wang, M. Yao, Y. Niu, C. Wang, Nonlinear dynamics of three-layer microplates: simultaneous presence of the micro-scale and imperfect effects, Eur. Phys. J. Plus 139 (2024) 446, https://doi.org/10.1140/epjp/s13360-024-05255-3.

[37] Q. Cen, Z. Xing, Q. Wang, L. Li, Z. Wang, Z. Wu, L. Liu, Molding simulation of airfoil foam sandwich structure and interference optimization of foam-core, Chin. J. Aeronaut. 37 (10) (2024) 325–338, https://doi.org/10.1016/j.cja.2024.08.025.

[38] Y. Yu, T. Fu, S. Wang, C. Yang, Dynamic response of novel sandwich structures with 3D sinusoid-parallel-hybrid honeycomb auxetic cores: the cores based on negative Poisson's ratio of elastic jump, Eur. J. Mech. A, Solids 109 (2025) 105449, https://doi.org/10.1016/j.euromechsol.2024.105449.

[39] K. Liu, S. Zong, Y. Li, Z. Wang, Z. Hu, Z. Wang, Structural response of the U-type corrugated core sandwich panel used in ship structures under the lateral quasi-static compression load, Mar. Struct. 84 (2022) 103198, https://doi.org/10.1016/j.marstruc.2022.103198.

[40] T. Fu, X. Hu, C. Yang, Impact response analysis of stiffened sandwich functionally graded porous materials doubly-curved shell with re-entrant honeycomb auxetic core, Appl. Math. Model. 124 (2023) 553–575, https://doi.org/10.1016/j.apm.2023.08.024.

[41] C. Wang, Z. Song, H. Fan, Novel evidence theory-based reliability analysis of functionally graded plate considering thermal stress behavior, Aerosp. Sci. Technol. 146 (2024) 108936, https://doi.org/10.1016/j.ast.2024.108936.

[42] J. Zhang, C. Zhang, Using viscoelastic materials to mitigate earthquake-induced pounding between adjacent frames with unequal height considering soil-structure interactions, Soil Dyn. Earthq. Eng. 172 (2023) 107988, https://doi.org/10.1016/j.soildyn.2023.107988.

[43] A. Robaldo, E. Carrera, A. Benjeddou, A unified formulation for finite element analysis of piezoelectric adaptive plates, Comput. Struct. 84 (22) (2006) 1494–1505, https://doi.org/10.1016/j.compstruc.2006.01.029.

[44] M. Cinefra, E. Carrera, S. Valvano, Variable kinematic shell elements for the analysis of electro-mechanical problems, Mech. Adv. Mat. Struct. 22 (1–2) (2015) 77–106, https://doi.org/10.1080/15376494.2014.908042.

[45] A.J.M. Ferreira, A.L. Araújo, A.M.A. Neves, J.D. Rodrigues, E. Carrera, M. Cinefra, C.M. Mota Soares, A finite element model using a unified formulation for the analysis of viscoelastic sandwich laminates, Composites, Part B, Eng. 45 (1) (2013) 1258–1264, https://doi.org/10.1016/j.compositesb.2012.05.012.

[46] A. Alaimo, C. Orlando, S. Valvano, Analytical frequency response solution for composite plates embedding viscoelastic layers, Aerosp. Sci. Technol. 92 (2019) 429–445, https://doi.org/10.1016/j.ast.2019.06.021.

[47] M. D'Ottavio, A. Krasnobrizha, E. Valot, O. Polit, R. Vescovini, L. Dozio, Dynamic response of viscoelastic multiple-core sandwich structures, J. Sound Vib. 491 (2021) 115753, https://doi.org/10.1016/j.jsv.2020.115753.

[48] A.R. Sánchez-Majano, R. Azzara, A. Pagani, E. Carrera, Accurate stress analysis of variable angle tow shells by high-order equivalent-single-layer and layer-wise finite element models, Materials 14 (21) (2021), https://doi.org/10.3390/ma14216486.

[49] A. Pagani, E. Zappino, F. Bracaglia, R. Masia, E. Carrera, Thermal stress analysis of variable angle tow composite plates through high-order structural models, Compos. Struct. 327 (2024) 117668, https://doi.org/10.1016/j.compstruct.2023.117668.

[50] J.A. Moreira, F. Moleiro, A.L. Araújo, A. Pagani, Assessment of layerwise user-elements in Abaqus for static and free vibration analysis of variable stiffness composite laminates, Compos. Struct. 303 (2023) 116291, https://doi.org/10.1016/j.compstruct.2022.116291.

[51] R. Vescovini, L. Dozio, A variable-kinematic model for variable stiffness plates: vibration and buckling analysis, Compos. Struct. 142 (2016) 15–26, https://doi.org/10.1016/j.compstruct.2016.01.068.

[52] J.A. Moreira, F. Moleiro, A.L. Araújo, A. Pagani, Equivalent single layer and layer-wise models for flutter and buckling analysis of supersonic variable stiffness laminated composite plates, Thin-Walled Struct. 191 (2023) 111012, https://doi.org/10.1016/j.tws.2023.111012.

[53] A. Pagani, M. Petrolo, G. Colonna, E. Carrera, Dynamic response of aerospace structures by means of refined beam theories, Aerosp. Sci. Technol. 46 (2015) 360–373, https://doi.org/10.1016/j.ast.2015.08.005.

[54] A. Viglietti, E. Zappino, E. Carrera, Free vibration analysis of variable angle-tow composite wing structures, Aerosp. Sci. Technol. 92 (2019) 114–125, https://doi.org/10.1016/j.ast.2019.05.068.

[55] Z.-G. Song, F.-M. Li, Active aeroelastic flutter analysis and vibration control of supersonic composite laminated plate, Compos. Struct. 94 (2) (2012) 702–713, https://doi.org/10.1016/j.compstruct.2011.09.005.

[56] T.A. Guimarães, D.A. Rade, C.E. Cesnik, Active flutter suppression on composite tow steered panels based on piezoelectric actuation, in: 59th AIAA/ASCE/AHS/ASC Structures, Structural Dynamics, and Materials Conference, 2018, https://arc.aiaa.org/doi/abs/10.2514/6.2018-0188.

[57] J.A. Moreira, F. Moleiro, A.L. Araújo, A. Pagani, Analytical modeling of panel flutter and active control in supersonic variable stiffness composite laminates, Mech. Adv. Mat. Struct. 30 (5) (2023) 930–944, https://doi.org/10.1080/15376494.2022.2144970.

[58] I.K. Oh, I. Lee, Supersonic flutter suppression of piezolaminated cylindrical panels based on multifield layerwise theory, J. Sound Vib. 291 (3) (2006) 1186–1201, https://doi.org/10.1016/j.jsv.2005.07.033.

[59] J.A. Moreira, F. Moleiro, A.L. Araújo, A. Pagani, Active aeroelastic flutter control of supersonic smart variable stiffness composite panels using layerwise models, Compos. Struct. (2024) 118287, https://doi.org/10.1016/j.compstruct.2024.118287.

[60] J.A. Moreira, F. Moleiro, A.L. Araújo, Layerwise electro-elastic user-elements in Abaqus for static and free vibration analysis of piezoelectric composite plates, Mech. Adv. Mat. Struct. 29 (21) (2022) 3109–3121, https://doi.org/10.1080/15376494.2021.1886381.

[61] W.T. Koiter, A consistent first approximation in the general theory of thin elastic shells, in: Proceedings of First Symposium on the Theory of Thin Elastic Shells, North-Holland, Amsterdam, 1959, http://resolver.tudelft.nl/uuid:13cb5366-bbdc-4dd1-8514-951302217759.

[62] H. Akhavan, P. Ribeiro, Stability and bifurcations in oscillations of composite laminates with curvilinear fibres under a supersonic airflow, Nonlinear Dyn. 103 (4) (2021) 3037–3058, https://doi.org/10.1007/s11071-020-05838-6.

[63] L.-q. Ye, K. Ye, K. Jin, Y.-f. Zhang, Z.-y. Ye, Mechanism of single-mode panel flutter in low supersonic flow, Aerosp. Sci. Technol. 147 (2024) 109002, https://doi.org/10.1016/j.ast.2024.109002.

[64] Y.-Y. Chai, Z.-G. Song, F.-M. Li, Active aerothermoelastic flutter suppression of composite laminated panels with time-dependent boundaries, Compos. Struct. 179 (2017) 61–76, https://doi.org/10.1016/j.compstruct.2017.07.053.